Atmos. Chem. Phys., 8, 4759–4786, 2008
www.atmos-chem-phys.net/8/4759/2008/

Atmospheric Chemistry and Physics

Validation of ACE-FTS N_2O measurements

K. Strong[1], M. A. Wolff[1], T. E. Kerzenmacher[1], K. A. Walker[1,2], P. F. Bernath[2,3], T. Blumenstock[4], C. Boone[2], V. Catoire[5], M. Coffey[6], M. De Mazière[7], P. Demoulin[8], P. Duchatelet[8], E. Dupuy[2], J. Hannigan[6], M. Höpfner[4], N. Glatthor[4], D. W. T. Griffith[9], J. J. Jin[10], N. Jones[9], K. Jucks[11], H. Kuellmann[12], J. Kuttippurath[12,*], A. Lambert[13], E. Mahieu[8], J. C. McConnell[10], J. Mellqvist[14], S. Mikuteit[4], D. P. Murtagh[14], J. Notholt[12], C. Piccolo[15], P. Raspollini[16], M. Ridolfi[17], C. Robert[5], M. Schneider[4], O. Schrems[18], K. Semeniuk[10], C. Senten[7], G. P. Stiller[4], A. Strandberg[14], J. Taylor[1], C. Tétard[19], M. Toohey[1], J. Urban[14], T. Warneke[12], and S. Wood[20]

[1]Department of Physics, University of Toronto, Toronto, Ontario, Canada
[2]Department of Chemistry, University of Waterloo, Waterloo, Ontario, Canada
[3]Department of Chemistry, University of York, York, UK
[4]Forschungszentrum Karlsruhe and University of Karlsruhe, Institute for Meteorology and Climate Research (IMK), Karlsruhe, Germany
[5]Laboratoire de Physique et Chimie de L'Environment CNRS – Université d'Orléans, Orléans, France
[6]National Center for Atmospheric Research, Boulder, CO, USA
[7]Belgian Institute for Space Aeronomy, Brussels, Belgium
[8]Institute of Astrophysics and Geophysics, University of Liège, Liège, Belgium
[9]School of Chemistry, University of Wollongong, Wollongong, Australia
[10]Department of Earth and Space Science and Engineering, York University, Toronto, Ontario, Canada
[11]Harvard-Smithsonian Center for Astrophysics, Cambridge, MA, USA
[12]Institute for Environmental Physics, University of Bremen, Bremen, Germany
[13]Jet Propulsion Laboratory, California Institute of Technology, Pasadena, CA, USA
[14]Department of Radio and Space Science, Chalmers University of Technology, Gothenburg, Sweden
[15]Department of Physics, University of Oxford, Oxford, UK
[16]Institute of Applied Physics "Nello Carrara", National Research Center, Firenze, Italy
[17]Dipartimento di Chimica Fisica e Inorganica, Università di Bologna, Bologna, Italy
[18]Alfred Wegener Institute for Polar and Marine Research, Bremerhaven, Germany
[19]Laboratoire d'Optique Atmosphérique, Université des sciences et technologies de Lille, Villeneuve d'Ascq, France
[20]National Institute of Water and Atmospheric Research Ltd., Lauder, New Zealand
[*]now at: LMD/CNRS Ecole Polytechnique, Palaiseau Cedex, France

Received: 28 November 2007 – Published in Atmos. Chem. Phys. Discuss.: 21 February 2008
Revised: 20 June 2008 – Accepted: 25 June 2008 – Published: 19 August 2008

Abstract. The Atmospheric Chemistry Experiment (ACE), also known as SCISAT, was launched on 12 August 2003, carrying two instruments that measure vertical profiles of atmospheric constituents using the solar occultation technique. One of these instruments, the ACE Fourier Transform Spectrometer (ACE-FTS), is measuring volume mixing ratio (VMR) profiles of nitrous oxide (N_2O) from the upper troposphere to the lower mesosphere at a vertical resolution of about 3–4 km. In this study, the quality of the ACE-FTS version 2.2 N_2O data is assessed through comparisons with coincident measurements made by other satellite, balloon-borne, aircraft, and ground-based instruments. These consist of vertical profile comparisons with the SMR, MLS, and MIPAS satellite instruments, multiple aircraft flights of ASUR, and single balloon flights of SPIRALE and FIRS-2, and partial column comparisons with a network of ground-based Fourier Transform InfraRed spectrometers (FTIRs). Between 6 and 30 km, the mean absolute differences for the satellite comparisons lie between −42 ppbv and +17 ppbv, with most within ±20 ppbv. This corresponds to relative deviations from the mean that are within ±15%, except for comparisons with MIPAS near 30 km, for which they are as large as 22.5%. Between 18 and 30 km, the mean absolute differences for the satellite comparisons are generally

Correspondence to: K. Strong
(strong@atmosp.physics.utoronto.ca)

Published by Copernicus Publications on behalf of the European Geosciences Union.

within ±10 ppbv. From 30 to 60 km, the mean absolute differences are within ±4 ppbv, and are mostly between −2 and +1 ppbv. Given the small N_2O VMR in this region, the relative deviations from the mean are therefore large at these altitudes, with most suggesting a negative bias in the ACE-FTS data between 30 and 50 km. In the comparisons with the FTIRs, the mean relative differences between the ACE-FTS and FTIR partial columns (which cover a mean altitude range of 14 to 27 km) are within ±5.6% for eleven of the twelve contributing stations. This mean relative difference is negative at ten stations, suggesting a small negative bias in the ACE-FTS partial columns over the altitude regions compared. Excellent correlation (R=0.964) is observed between the ACE-FTS and FTIR partial columns, with a slope of 1.01 and an intercept of −0.20 on the line fitted to the data.

1 Introduction

Nitrous oxide (N_2O) is an important atmospheric constituent, as it is the primary source gas for nitrogen oxides in the stratosphere, a useful dynamical tracer, and an efficient greenhouse gas. N_2O has many surface and near-surface sources, with approximately equal contributions from natural and anthropogenic emissions. Natural sources include biological nitrogen cycling in the oceans and soils and oxidation of NH_3, while anthropogenic sources include chemical conversion of nitrogen in fertilizers into N_2O, biomass burning, cattle, and some industrial activities (IPCC, 2007). It is the only long-lived atmospheric tracer of human perturbations of the global nitrogen cycle (Holland et al., 2005). There are large uncertainties in N_2O source strengths derived from emissions inventories, with estimates of the total source strength varying by ±50% (McLinden et al., 2003, and references therein). Tropospheric N_2O is transported through the tropical tropopause into the stratosphere, where approximately 90% is destroyed by photolysis at wavelengths from 185 to 220 nm, which creates N_2 and O. The remaining 10% is destroyed by reaction with $O(^1D)$. The latter has two channels, one of which generates two NO molecules and serves as the source for stratospheric nitrogen oxides, which participate in catalytic destruction of ozone (Bates and Hays, 1967; Crutzen, 1970; McElroy and McConnell, 1971).

While N_2O is well-mixed in the troposphere, its concentration decays with altitude in the stratosphere due to the reactions noted above. Its photochemical lifetime varies from approximately 100 years at 20 km and below, to 1 year at 33 km and 1 month at 40 km (Brasseur and Solomon, 2005). As these lifetimes are longer than dynamical time scales, the global distribution of N_2O is primarily governed by the Brewer-Dobson circulation. This makes it a useful tracer in the stratosphere, both as a diagnostic tool in atmospheric models (Mahlman et al., 1986; Holton, 1986; Bregman et al., 2000; Plumb and Ko, 1992; Avallone and Prather, 1997; Sankey and Shepherd, 2003) and for the interpretation of observational data. For example, N_2O has been used in numerous studies of polar vortex dynamics and chemistry (e.g., Proffitt et al., 1989, 1990, 1992; Müller, 1996; Bremer et al., 2002; Urban et al., 2004), the tropical pipe (e.g., Plumb, 1996; Murphy et al., 1993; Volk et al., 1996; Minschwaner et al., 1996; Avallone and Prather, 1996), transport and chemistry in the upper troposphere/lower stratosphere (e.g., Boering et al., 1994; Hegglin et al., 2006), and global transport processes (e.g., Randel et al., 1993, 1994).

Radiatively, N_2O is a long-lived greenhouse gas (Yung et al., 1976; Ramanathan et al., 1985). It has a global warming potential of 289 over 20 years, and a global average radiative forcing due to increases in N_2O since the pre-industrial era of $0.16\pm0.02\,Wm^{-2}$, making it the fourth most important trace gas contributing to positive forcing (IPCC, 2007). Global surface concentrations of atmospheric N_2O are currently increasing at about 0.26% per year, and have risen from a pre-industrial value of about 270 ppbv to 319 ppbv in 2005, due to an increase of 40–50% in surface emissions over that period due to human activities (Battle et al., 1996; Flückiger et al., 1999; Zander et al., 2005; Hirsch et al., 2006; WMO, 2006; IPCC, 2007, and references therein). There is a hemispheric difference in N_2O, with about 0.8 ppbv more in the northern hemisphere, which is the source of approximately 60% of the emissions (Brasseur and Solomon, 2005).

Global distributions of N_2O have been measured from space since 1979, when the Stratospheric and Mesospheric Sounder (SAMS) on Nimbus 7 began operations (Drummond et al., 1980; Jones and Pyle, 1984; Jones et al., 1986). SAMS used an infrared pressure modulator radiometer to measure thermal emission from the limb at 7.8 μm, from which stratospheric N_2O profiles were retrieved until 1983. This was followed by the Improved Stratospheric and Mesospheric Sounder (ISAMS) and the Cryogenic Limb Array Etalon Spectrometer (CLAES) on the Upper Atmosphere Research Satellite (UARS). ISAMS also used pressure modulator radiometers, operating from 4.6 to 16.3 μm, and provided N_2O profiles between October 1991 and July 1992 (Taylor et al., 1993; Ruth et al., 1994; Remedios et al., 1996). CLAES also measured N_2O using thermal limb emission, from 3.5 to 13 μm, between October 1991 and May 1993 (Roche et al., 1993, 1996). The Atmospheric Trace Molecule Spectroscopy (ATMOS) instrument, flown on four Space Shuttle missions, first on Spacelab-3 in 1985 and subsequently on Atmospheric Laboratory for Applications and Science (ATLAS)-1, -2, and -3 in 1992, 1993, and 1994, made the first infrared solar occultation measurements of N_2O from space (Abrams et al., 1996; Gunson et al., 1996; Michelsen et al., 1998; Irion et al., 2002). Also flown on ATLAS-3, in 1994, was the CRyogenic Infrared Spectrometers and Telescopes for the Atmosphere (CRISTA), which used four spectrometers to measure emission in the limb at mid-infrared (4–14 μm) and far-infrared (15–71 μm) wavelengths (Offermann et al., 1999; Riese et al., 1999). The Improved Limb

Atmospheric Spectrometer (ILAS) and ILAS-II instruments on the Advanced Earth Observing Satellite (ADEOS) and ADEOS-II, respectively, both measured N_2O using infrared solar occultation. ILAS made measurements from September 1996 to June 1997 (Kanzawa et al., 2003; Khosrawi et al., 2004), while ILAS-II operated for eight months in 2003 (Ejiri et al., 2006; Khosrawi et al., 2006).

There are currently four satellite instruments in orbit measuring N_2O. One of these is the Atmospheric Chemistry Experiment Fourier Transform Spectrometer (ACE-FTS) on SCISAT, launched in 2003 (Bernath et al., 2005). The others are the Sub-Millimetre Radiometer (SMR) on Odin, launched in 2001 (Murtagh et al., 2002; Urban et al., 2005a,b, 2006), the Michelson Interferometer for Passive Atmospheric Sounding (MIPAS) on Envisat, launched in 2002 (Fischer et al., 2008), and the Microwave Limb Sounder (MLS) on the Aura satellite (Waters et al., 2006; Lambert et al., 2007), launched in 2004. These are described in more detail below.

The objective of this study is to assess the quality of the ACE-FTS version 2.2 N_2O data, prior to its public release, through comparisons with coincident measurements. The paper is organized as follows. In Sect. 2, the ACE mission and the N_2O retrievals are briefly described. Section 3 outlines the methodology used to compare and present the validation results. In Sect. 4, the results of vertical profile comparisons with the SMR, MLS, and MIPAS satellite instruments are discussed. Section 5 focuses on the results of comparisons with data from the ASUR (Airborne SUbmillimeter wave Radiometer) aircraft flights and from the SPIRALE (SPectroscopie Infra-Rouge d'Absorption par Lasers Embarqués) and FIRS-2 (Far-InfraRed Spectrometer-2) balloon flights. Partial column comparisons with a network of ground-based Fourier Transform InfraRed spectrometers (FTIRs) are presented in Sect. 6. Finally, the results are summarized and conclusions regarding the quality of the ACE-FTS version 2.2 N_2O data are given in Sect. 7.

2 The ACE mission and ACE-FTS N_2O retrievals

The Atmospheric Chemistry Experiment has been in orbit since its launch on 12 August 2003. ACE is a Canadian-led satellite mission, also known as SCISAT, which carries two instruments, the ACE-FTS (Bernath et al., 2005) and the Measurement of Aerosol Extinction in the Stratosphere and Troposphere Retrieved by Occultation (ACE-MAESTRO) (McElroy et al., 2007). Both instruments record solar occultation spectra, ACE-FTS in the infrared (IR), and MAESTRO in the ultraviolet-visible-near-IR, from which vertical profiles of atmospheric trace gases, temperature, and aerosol extinction are retrieved. The SCISAT spacecraft is in a circular orbit at 650-km altitude, with a 74° inclination angle (Bernath et al., 2005), providing up to 15 sunrise and 15 sunset solar occultations per day. The choice of orbital parameters results in coverage of the tropics, mid-latitudes and polar regions with an annually repeating pattern, and a sampling frequency that is greatest over the Arctic and Antarctic. The primary scientific objectives of the ACE mission are: (1) to understand the chemical and dynamical processes that control the distribution of ozone in the stratosphere and upper troposphere, particularly in the Arctic; (2) to explore the relationship between atmospheric chemistry and climate change; (3) to study the effects of biomass burning on the free troposphere; and (4) to measure aerosols and clouds to reduce the uncertainties in their effects on the global energy balance (Bernath et al., 2005; Bernath, 2006, and references therein).

ACE-FTS measures atmospheric spectra between 750 and 4400 cm^{-1} (2.2–13 μm) at 0.02 cm^{-1} resolution (Bernath et al., 2005). Profiles as a function of altitude for pressure, temperature, and over 30 trace gases are retrieved from these spectra. The details of ACE-FTS processing are described in Boone et al. (2005). Briefly, a non-linear least squares global fitting technique is employed to analyze selected microwindows (0.3–30 cm^{-1} wide portions of the spectrum containing spectral features for the target molecule). Prior to performing volume mixing ratio (VMR) retrievals, pressure and temperature as a function of altitude are determined through the analysis of CO_2 lines in the spectra. Forward model calculations employ the spectroscopic constants and cross-section measurements from the HITRAN 2004 line list (Rothman et al., 2005). First-guess profiles are based on ATMOS measurements, but the retrievals are not sensitive to this a priori information.

The ACE-FTS instrument collects measurements every 2 s, which yields a typical altitude sampling of 3–4 km within an occultation, neglecting the effects of refraction that compress the spacing at low altitudes. The altitude coverage of the measurements extends from the upper troposphere to as high as 150 km, depending on the constituent. Note that the altitude spacing can range from 1.5 to 6 km, depending on the geometry of the satellite's orbit for a given occultation. The actual altitude resolution achievable with the ACE-FTS is limited to about 3–4 km, a consequence of the instrument's field-of-view (1.25-mrad-diameter aperture and 650-km altitude). Atmospheric quantities are retrieved at the measurement heights. For the purpose of generating calculated spectra (i.e., performing forward model calculations), quantities are interpolated from the measurement grid onto a standard 1-km grid using piecewise quadratic interpolation. The comparisons in this work use the ACE-FTS VMR profiles on the 1-km grid.

N_2O is one of the 14 primary target species for the ACE mission. A total of 69 microwindows are used in the version 2.2 ACE-FTS retrievals for N_2O. They are in the wavenumber ranges 1120–1280, 1860–1951, 2180–2240, 2440–2470, and 2510–2600 cm^{-1}. The altitude range for the retrieval extends from 5 to 60 km. The primary interfering species in the microwindow set are CO_2, O_3, and CH_4. These interfering species are retrieved simultaneously with N_2O. The

Table 1. Summary of the correlative datasets used for the statistical and individual profile comparisons with ACE-FTS N_2O.

Instrument (retrieval code)	Comparison period	Comparison location	Vertical range and resolution	Coincidence criteria	Number of coincidences
SMR (Chalmers v2.1)	21 February 2004–30 November 2006	83° S–83° N	12–60 km at ∼1.5 km	±12 h, ±1° lat, ±8° long	1099
MLS (version 2.2)	16 September 2004–26 February 2007	82° S–82° N	14–50 km at 4–6 km	±12 h, ±1° lat, ±8° long	6876
MIPAS ESA product (version 4.62)	21 February 2004–26 March 2004	20–85° N	6–60 km at 3–4 km	±6 h, 300 km	141
MIPAS IMK-IAA product (version 9)	21 February 2004–25 March 2004	30–90° N	6–60 km at 3–6 km	±9 h, 800 km $\pm 3\times10^{-6}$ km^2 kg^{-1} s^{-1} at 475 K	372 outside vortex 114 inside vortex
ASUR	24 January 2005–7 February 2005	60–70° N	18–46 km at 8–16 km	±12 h, 1000 km	17
SPIRALE	20 January 2006	67.6° N, 21.55° E	15–26 km at several m	13 h, 413 km	1
FIRS-2	24 January 2007	67.27° N, 27.29° E	13–31 km at 1 km	26 h, 481 km	1

precision of the ACE-FTS N_2O VMRs is defined as the 1σ statistical fitting errors from the least-squares process, assuming a normal distribution of random errors (Boone et al., 2005). We have examined these fitting errors for the ACE-FTS N_2O profiles used in the comparisons with MLS (Sect. 4.2), and found that the median value is <3% from 5–45 km, increasing to 17% at 60 km, while the mean value is <4% from 5–35 km, and oscillating above this due to some outliers in the individual percent fitting errors. While these fitting errors provide some useful information regarding the precision of the ACE-FTS measurements, they do not represent complete error estimates. Work is in progress to generate full error budgets for all of the ACE-FTS data products, but that information is not currently available.

To date, ACE-FTS N_2O profiles have been compared with MLS data (Froidevaux et al., 2006; Lambert et al., 2007; Toohey and Strong, 2007), and partial columns have been compared with those retrieved using the Portable Atmospheric Research Interferometric Spectrometer for the Infrared (PARIS-IR), a ground-based adaptation of ACE-FTS, during the spring 2004 Canadian Arctic ACE validation campaign (Sung et al., 2007).

3 Validation approach

The comparisons shown in this work include ACE-FTS data from 21 February 2004 (the start of the ACE Science Operations phase) through to 26 February 2007. The coincidence criteria for each correlative dataset were determined in consultation with the teams involved, striving for consistency insofar as possible. The location for each ACE occultation is defined as the latitude, longitude and time of the 30-km tangent point (calculated geometrically), and it is this value that was used in searching for coincidences. Because N_2O is a long-lived and well-mixed constituent, it was possible to use relatively relaxed temporal and spatial coincidence criteria, thereby providing good statistics for the comparisons. For the global satellite datasets, available for SMR and MLS, the coincidence criteria were defined as ±12 h, ±1° latitude and ±8° longitude, as used by Lambert et al. (2007) in the validation of MLS N_2O measurements. Correlative data for MIPAS were only available for a two-month period in early 2004 for northern mid- and high latitudes, and for these, slightly tighter criteria were defined. For the ASUR aircraft measurements, obtained during several flights, the coincidence criteria were defined as ±12 h and 1000 km. For the statistical comparisons, unless otherwise noted, multiple counting of profiles was allowed, so that if n validation measurements met the criteria with respect to a single ACE-FTS occultation, then these would be included as n coincidences and the

ACE-FTS measurement would be counted n times. Balloon-based single profile measurements by SPIRALE and FIRS-2 obtained within ±26 h and 500 km of ACE occultations were included in the comparisons. Finally, for the ground-based FTIRs, the criteria were set at ±24 h and 1000 km for all but two stations (see Sect. 6), to provide a meaningful number of coincidences. Table 1 summarizes the correlative datasets, comparison periods, temporal and spatial coincidence criteria, and number of coincidences for the statistical and individual profile comparisons. Information about the FTIR stations and comparisons is provided in Tables 2 and 3 in Sect. 6.

The SMR, MLS, MIPAS, and FIRS-2 VMR profiles all have vertical resolutions that are similar to that of ACE-FTS, and so no smoothing was applied to these data. These correlative profiles were linearly interpolated onto the 1-km ACE altitude grid. MLS profiles, reported on pressure levels, were mapped onto the 1-km altitude grid of ACE by interpolating in log pressure each MLS profile onto the retrieved pressure profile of the coincident ACE-FTS observation. The aircraft-based ASUR instrument has lower vertical resolution than ACE-FTS, so the ACE-FTS profiles were convolved with the ASUR averaging kernels. The balloon-borne SPIRALE VMR profile was obtained at significantly higher vertical resolution than ACE-FTS, and so was convolved with triangular functions having full width at the base equal to 3 km and centered at the tangent height of each occultation (see Eq. 1 of Dupuy et al., 2008). This approach simulates the smoothing effect of the ACE-FTS field-of-view, as discussed by Dupuy et al. (2008). The resulting smoothed profiles were then interpolated onto the 1-km grid. Finally, for the comparisons with the ground-based FTIR measurements, which have significantly lower vertical resolution, the ACE-FTS profiles were smoothed by the appropriate FTIR averaging kernels to account for the different vertical sensitivities of the two measurement techniques. The method of Rodgers and Connor (2003) was followed and Eq. (4) from their paper was applied, using the a priori profile and the averaging kernel matrix appropriate for each FTIR. Partial columns over specified altitude ranges were then calculated for both ACE-FTS and the FTIRs, as described in Sect. 6, and these were used in the comparisons.

Co-located pairs of vertical VMR profiles from ACE-FTS and each validation experiment (referred to as VAL in text and figures below) were identified using the appropriate temporal and spatial coincidence criteria. Then the following procedure was applied to the vertical profile measurements used in this assessment, with some modifications for the individual profile comparisons (SPIRALE and FIRS-2) and the FTIR partial column comparisons (see Sect. 5 and Sect. 6 for details).

(a) Calculate the mean profile of the ensemble for ACE-FTS and the mean profile for VAL, along with their standard deviations calculated from the individual profiles for each altitude. These mean profiles are plotted as solid lines, with $\pm 1\sigma$ as dashed lines, in panel (a) of the comparison figures discussed below. The standard error on the mean, also known as the uncertainty in the mean, is calculated as $\sigma(z)/\sqrt{N(z)}$, where $N(z)$ is the number of points used to calculate the mean at a particular altitude z, and is included as error bars on the lines in panel (a). Note: in some cases, these error bars, as well as those in panels (b) and (c) (see below) may be small and difficult to distinguish.

(b) Calculate the profile of the mean absolute difference, ACE-FTS − VAL, and the standard deviation of the individual differences of all coincident pairs as a function of altitude. (Note that the term "absolute", as used in this work, refers to differences between the compared values and not to absolute values in the mathematical sense.) To do this, the differences are first calculated for each pair of profiles at each altitude, and then averaged to obtain the mean absolute difference at altitude z:

$$\Delta_{\text{abs}}(z) = \frac{1}{N(z)} \sum_{i=1}^{N(z)} [\text{ACE}_i(z) - \text{VAL}_i(z)] \quad (1)$$

where $N(z)$ is the number of coincidences at z, $\text{ACE}_i(z)$ is the ACE-FTS VMR at z for the ith coincident pair, and $\text{VAL}_i(z)$ is the corresponding VMR for the validation instrument. This mean absolute difference is plotted as a solid line in panel (b) of the comparison figures below, with $\pm 1\sigma$ as dashed lines. Error bars are also included in these figures. For the statistical comparisons involving multiple coincident pairs (SMR, MLS, MIPAS, ASUR), these error bars again represent the uncertainty in the mean. For individual profile comparisons (SPIRALE, FIRS-2), these error bars represent the combined random error, computed as the root-sum-square error of the ACE-FTS fitting error and the error provided for VAL.

(c) Calculate the profile of the mean relative difference, as a percentage, defined using:

$$\begin{aligned} \Delta_{\text{rel}}(z) &= 100\% \times \frac{1}{N(z)} \sum_{i=1}^{N(z)} \frac{[\text{ACE}_i(z) - \text{VAL}_i(z)]}{[\text{ACE}_i(z) + \text{VAL}_i(z)]/2} \\ &= 100\% \times \frac{1}{N(z)} \sum_{i=1}^{N(z)} \frac{[\text{ACE}_i(z) - \text{VAL}_i(z)]}{\text{MEAN}_i(z)} \end{aligned} \quad (2)$$

where $\text{MEAN}_i(z)$ is the mean of the two coincident profiles at z for the ith coincident pair. Panel (c) of the comparison figures presents the mean relative difference as a solid cyan line. In addition, the relative deviation from the mean is calculated for the statistical comparisons using:

$$\Delta_{\text{mean}}(z) = 100\% \times \frac{\frac{1}{N(z)}\sum_{i=1}^{N(z)}[\text{ACE}_i(z) - \text{VAL}_i(z)]}{\frac{1}{N(z)}\sum_{i=1}^{N(z)}[\text{ACE}_i(z) + \text{VAL}_i(z)]/2}$$
$$= 100\% \times \frac{1}{N(z)}\sum_{i=1}^{N(z)}\frac{[\text{ACE}_i(z) - \text{VAL}_i(z)]}{\text{MEAN}(z)}$$
$$= 100\% \times \frac{\Delta_{abs}(z)}{\text{MEAN}(z)} \quad (3)$$

where MEAN(z) is the mean of all pairs of coincident profiles at z, which is equivalent to the mean of the average ACE-FTS VMR at z and average VAL VMR at z. This is plotted as the solid dark blue line in panel (c). The relative standard deviation is calculated as the standard deviation on $\Delta_{\text{abs}}(z)$ from step (b) divided by MEAN(z), and is plotted as dashed lines ($\pm 1\sigma$), with the corresponding relative standard error on the mean included as error bars. In the discussions of relative comparisons below, it is $\Delta_{\text{mean}}(z)$ that is primarily used; this reduces the impact of very small denominators and noisy data in Eq. (2), which can make $\Delta_{\text{rel}}(z)$ very large (von Clarmann, 2006).

(d) For the statistical comparisons, calculate the relative standard deviations on each of the ACE-FTS and VAL mean profiles calculated in step (a). For individual profile comparisons, the relative values of the ACE-FTS fitting error and the error for VAL are determined instead. These results are plotted in panel (d) of the comparison figures, with selected values of the number of coincident pairs given as a function of altitude on the right-hand y-axis for the statistical comparisons. For clarity, numbers are not given for all levels.

4 Comparisons with satellite measurements

4.1 SMR

The Sub-Millimetre Radiometer (SMR), launched on Odin in February 2001, has four tunable heterodyne radiometers that are used to detect thermal limb emission from atmospheric molecules between 486 and 581 GHz. Odin is in a sun-synchronous, near-terminator orbit at an altitude of ~600 km and an inclination of 97.8° (Murtagh et al., 2002). SMR observes a thermal emission line of N_2O in the limb at 502.3 GHz, and measurements of near-global fields of N_2O are performed on a time-sharing basis with other observation modes on roughly one day out of three, based on 14–15 orbits per day and 40–60 limb scans per orbit. Algorithms based on the optimal estimation method (Rodgers, 2000) are used for SMR profile retrievals. The latest level 2 version is Chalmers v2.1. N_2O profile information is retrieved in the stratosphere between ~12 and ~60 km with an altitude resolution of ~1.5 km (in the lower stratosphere, degrading above) and a corresponding single profile precision smaller than 30 ppbv (10–15% below 30 km) (Urban et al., 2006). The horizontal resolution is of the order of 300 km, determined by the limb path in the tangent layer. The satellite motion leads to an uncertainty of the mean profile position of similar magnitude. The SMR N_2O data are validated in the range ~15–50 km. The systematic error is estimated to be better than 12 ppbv at altitudes above ~20 km and increases up to values of 35 ppbv (~10–15%) below (Urban et al., 2005b), consistent with results obtained in the validation studies showing, for example, a good overall agreement within 4–7 ppbv with data from MIPAS (European Space Agency (ESA) operational processor version 4.61) (Urban et al., 2005a, 2006).

For this study, only SMR profiles of good quality (assigned Quality flag=0 or 4) were used. The measurement response, provided in the SMR level 2 files for each retrieval altitude, was required to be larger than 0.9 as recommended by Urban et al. (2005a), in order to exclude altitude ranges where a priori information used by the retrieval algorithm for stabilization contributes significantly to the retrieved mixing ratios. The comparisons used coincidence criteria of ±12 h, ±1° latitude, and ±8° longitude, and included data from 21 February 2004 to 30 November 2006. This yields 1099 multiple coincident pairs, allowing investigation of the latitudinal behaviour of ACE-FTS–SMR comparisons. In order to exclude extreme outliers, relative differences over 1000% were not included when deriving the mean of the relative differences. This excluded about 2% of the data from the comparison, removing 984 altitudes between 21 and 59 km, and leaving 45 690 altitudes for which the relative differences were less than 1000%.

The results of the comparison between ACE-FTS and SMR profiles between 83° S and 83° N (nominally 90° S–90° N) are shown in Fig. 1. Excellent agreement is seen between the mean N_2O VMR profiles (panel (a)) and in the mean absolute differences (panel (b)) between 15 and 50 km, which is the validated altitude range for SMR N_2O. From 15–50 km, the mean absolute difference is better than −10 ppbv, and is better than −5 ppbv for all but four levels in this altitude range, with ACE-FTS values generally being the smaller of the two, by −2.4 ppbv on average. Comparisons are also shown outside the validated range for SMR (13–15 km and 50–57 km): between 50 and 57 km, the SMR profiles decrease rapidly, leading to larger differences relative to ACE-FTS, varying from −1.5 ppbv at 50.5 km to +1.0 ppbv at 56.5 km.

Figure 1c illustrates the difficulty of obtaining useful information from the mean relative difference defined in Eq. (2) for a species such as N_2O, whose VMR decreases to very small values (typically a few ppbv in the upper stratosphere), and for which there are some coincident profiles whose values for each instrument are of the same magnitude but opposite sign. In some cases, the denominator in Eq. (2) is zero or close to zero, resulting in very large values. These values strongly affect the mean relative difference, although the number of these cases is relatively small; thus these

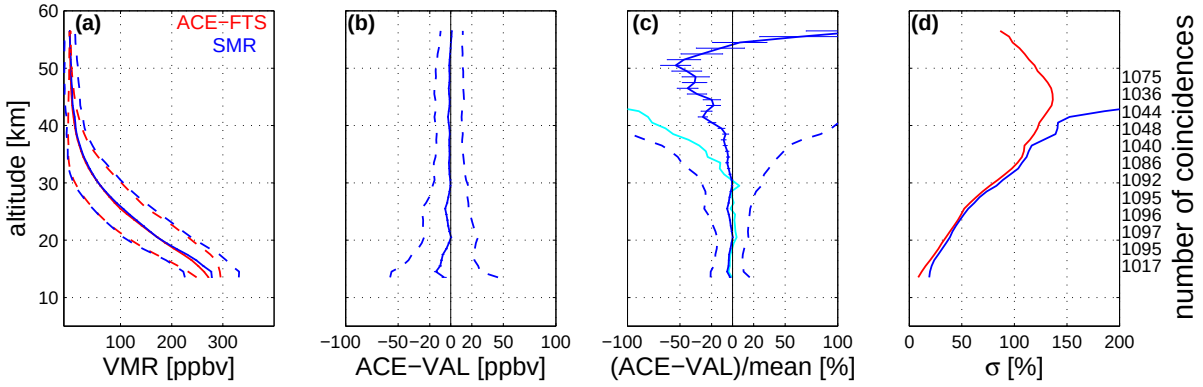

Fig. 1. Comparison of ACE-FTS and SMR N_2O VMR profiles from 90° S–90° N. **(a)** Mean profiles for ACE-FTS (red solid line) and SMR (blue solid line). These mean profiles $\pm 1\sigma$ standard deviation are plotted as dashed lines, and the standard errors in the mean ($\sigma/\sqrt{N}$) are included as error bars on the mean profiles. **(b)** Mean absolute difference profile (solid line) with $\pm 1\sigma$ standard deviation (dashed lines) and the standard error in the mean (error bars). **(c)** Relative deviation from the mean, as a percentage, calculated using Eq. (3) (blue solid line) with $\pm 1\sigma$ relative standard deviation (blue dashed lines) and the relative standard error in the mean (error bars). The profile of the mean relative difference calculated using Eq. (2) is also shown (cyan solid line). **(d)** Relative standard deviations for the mean profiles shown in (a). The number of coincident pairs at selected altitudes is given on the right-hand y-axis.

extremely large values are excluded as stated above. However, the mean relative difference is still affected by the noisiness of SMR data in the upper stratosphere and lower mesosphere, as seen in the relative standard deviation on SMR in Fig. 1d. In the upper stratosphere and lower mesosphere where the ACE-FTS N_2O VMR is small and the SMR N_2O VMR is noisy, the denominator in the expression $[\mathrm{ACE}_i(z) - \mathrm{VAL}_i(z)]/\mathrm{MEAN}_i(z)$ is close to half of the SMR VMR and the numerator is close to the SMR VMR, making the ratio approach 200%. As a consequence, the mean relative difference is not a good indicator of the agreement between ACE-FTS and SMR at higher altitudes, although it is better than −7% between 15 and 30 km. Figure 1c thus also includes the relative deviation from the mean, as defined in Eq. (3); this shows better agreement between ACE-FTS and SMR, to better than −20%, and to −4% on average, between 15 and 40 km. Between 40 and 50 km, the relative deviation from the mean is as large as −44%, with ACE-FTS consistently smaller. Above 50 km, as the SMR N_2O VMRs decrease, the negative bias of ACE-FTS decreases, becoming a positive bias at 54 km, with a maximum value of +127% at 56.5 km. These large values of the relative deviation from the mean at high altitudes are due to the noisy data in this region, particularly for SMR, as can be seen in the large relative standard deviations on the mean profiles plotted in Fig. 1d.

The data shown in Fig. 1 have been subdivided into five latitude bands in Fig. 2: 60–90° N, 30–60° N, 30° S–30° N, 30–60° S, and 60–90° S. The latitudinal gradients in N_2O are small at the lower and higher altitudes, as can be seen when comparing the mean profiles for each zonal band. However, a clear latitudinal gradient can be seen in the mid-stratosphere; for example, at 30 km, the mean ACE-FTS VMR is 155 ppbv for 30° S–30° N, dropping in the mid-latitudes to 82 (63) ppbv for 30–60° S (N), and down to 35 ppbv in the polar regions of both hemispheres. Very similar behaviour is seen in the SMR mean profiles. The mean absolute differences are similar in the five bands, with ACE-FTS being consistently slightly smaller than SMR between 15 and 50 km, with the exception of a few levels in each case. These differences are again typically about −2 ppbv, with maximum values of −7 ppbv from 60–90° N, −18 ppbv from 30–60° N, −27 ppbv from 30° S–30° N (at 15.5 km with only 22 coincident pairs), −11 ppbv from 30–60° S, and −10 ppbv from 60–90° S. The mean relative differences remain less than 8% between 15 and 30 km, for all but two levels (−13% at 28.5 km for 60–90° S and −16% at 29.5 km for 60–90° N). There is more variability between the latitude bands in the relative deviations from the mean; these are typically better than 5% between 12 and 40 km, with maxima of −24% from 60–90° N, −29% from 30–60° N, −8% from 30° S–30° N, −40% from 30–60° S (at 12.5 km with only 25 coincident pairs (not labelled)), and −17% from 60–90° S. The relative deviations from the mean increase above 40 km, where the relative standard deviations for the individual mean profiles are also seen to reach values of 100% and larger.

4.2 MLS

The Microwave Limb Sounder (MLS) was launched on the Aura satellite in July 2004. It is in a sun-synchronous orbit at an altitude of 705 km and an inclination of 98°, with the ascending node crossing the equator at 13:45 local time (Waters et al., 2006). Global measurements are obtained daily from 82° S to 82° N, with 240 scans per orbit. Like SMR,

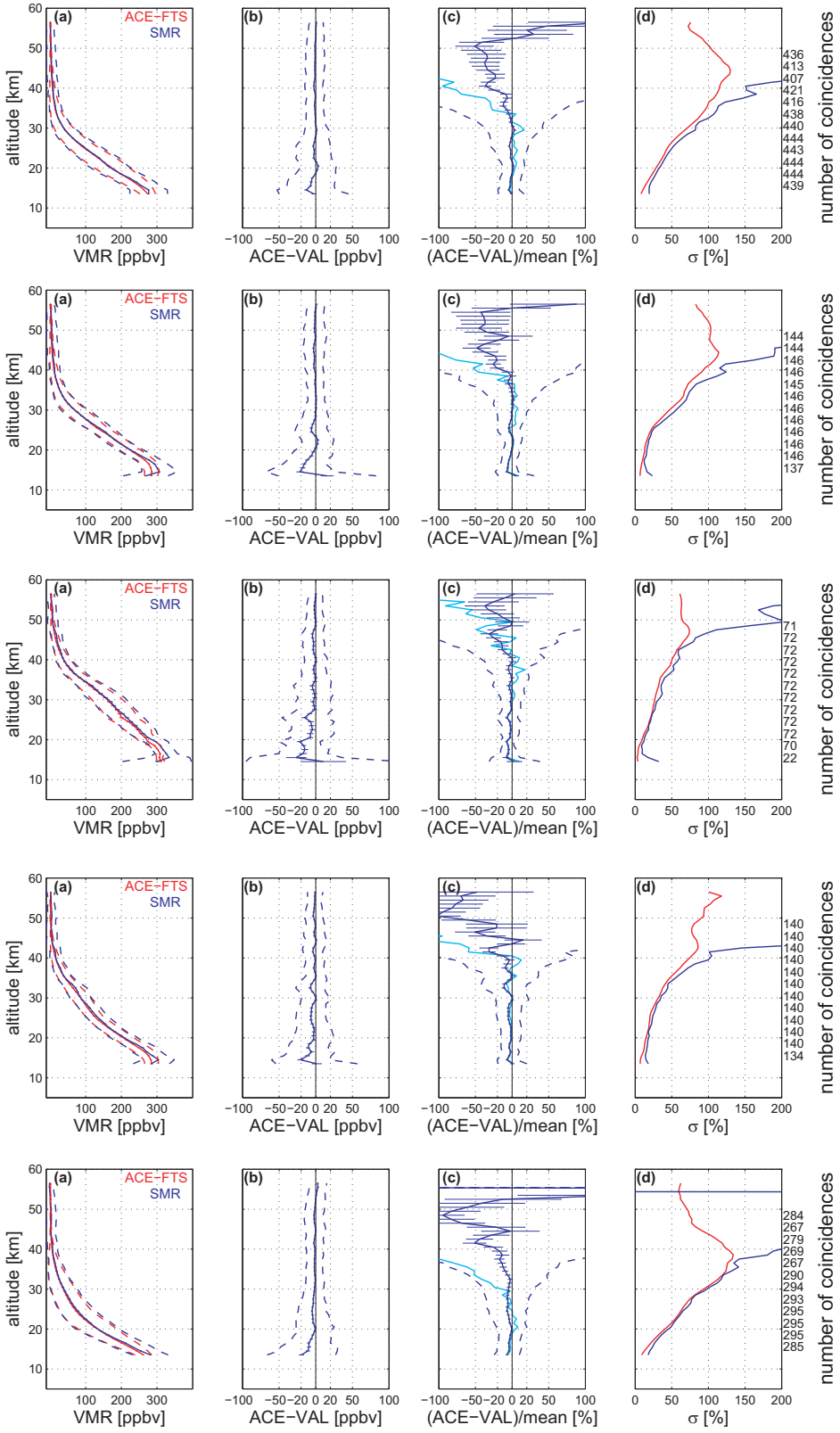

Fig. 2. Comparison of ACE-FTS and SMR N_2O VMR profiles in five latitude bands. Top row: 60–90° N, second row: 30–60° N, third row: 30° S–30° N, fourth row: 30–60° S, bottom row: 60–90° S. Panels **(a)**, **(b)**, **(c)** and **(d)** are the same as those in Fig. 1.

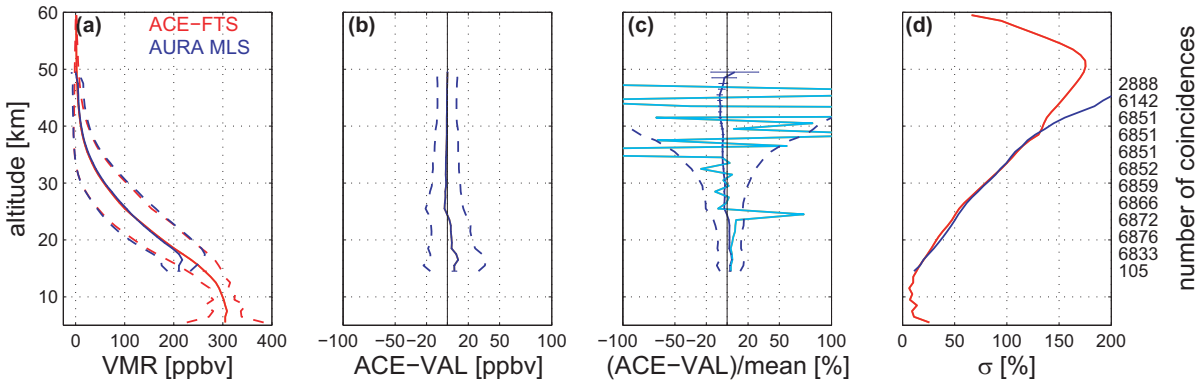

Fig. 3. Same as Fig. 1 but for comparisons between ACE-FTS and MLS from 90° S to 90° N.

MLS measures atmospheric thermal emission from the limb, using seven radiometers to provide coverage of five spectral regions between 118 GHz and 2.5 THz. Volume mixing ratio profiles of N_2O are retrieved from the thermal emission line at 652.83 GHz using the optimal estimation approach described by Livesey et al. (2006). The retrieval is performed on a pressure grid with six levels per decade for pressures greater than 0.1 hPa and three levels per decade for pressures less than 0.1 hPa. The vertical resolution for N_2O VMR profiles is 4–6 km, the along-track horizontal resolution is 300–600 km, and the recommended pressure range for the use of individual profiles is 100–1 hPa (Livesey et al., 2007).

For the comparisons in this work, MLS version 2.2 is used. Validation of the v2.2 N_2O data product is described by Lambert et al. (2007), while Froidevaux et al. (2006) discuss initial validation of MLS v1.5 data products, including N_2O. The precision of individual v2.2 N_2O profiles is estimated to be ∼13–25 ppbv (7–38%) for pressures between 100 and 4.6 hPa, while the accuracy is 3–70 ppbv (9–25%) over the same pressure range (Lambert et al., 2007). Initial comparisons between MLS v2.2 and ACE-FTS v2.2 N_2O indicated agreement in the mean percentage difference profiles to better than ±5% over 100–1 hPa, with MLS showing a low bias (within −5%) for pressures >32 hPa and a high bias (within +5%) for lower pressures. Analysis of the latitudinal behaviour of the mean absolute difference showed that MLS is consistently smaller than ACE-FTS at most latitudes for pressures between 100 and 32 hPa. Differences were somewhat smaller for ACE-FTS sunrise occultations than for sunset at 46–10 hPa.

Lambert et al. (2007) used an initial subset of the MLS v2.2 reprocessed data, which provided 1026 coincidences for the comparisons with ACE-FTS N_2O. These were obtained over 121 days between September 2004 and October 2006. The present study extends the analyses of Lambert et al. (2007), using data from 16 September 2004 through 26 February 2007, which includes 6876 pairs using coincidence criteria of ±12 h, ±1° latitude, ±8° longitude, and multiple counting. The MLS data used in this work are screened based on the recommended parameters: even values of the Status field, Quality values greater than 0.5, Convergence values less than 1.55, positive precision, and pressure levels between 100 and 1 hPa (Livesey et al., 2007; Lambert et al., 2007). ACE-FTS data were filtered by removing profiles flagged as Do Not Use (DNU) (see https://databace.uwaterloo.ca/validation/data_issues.php). For the period of MLS coincidences, this removed only one DNU occultation.

Figure 3 shows the results of the comparison between ACE-FTS and MLS profiles from 82° S and 82° N. Excellent agreement is seen over all altitudes, with the mean absolute difference between −3 and +10 ppbv from 15 to 50 km, with differences of 1 ppbv on average over this altitude range, and better than 4 ppbv above 20 km. The mean relative difference exhibits large oscillations, which result from some coincident profiles whose values for each instrument are of the same magnitude but opposite sign, leading to extremely small (or infinitesimal) values of the calculated mean. Dividing by infinitesimal values in (Eq. 2) leads to very large outlying values, as has been confirmed by an examination of all the individual profiles of $\mathrm{ACE}_i(z) - \mathrm{VAL}_i(z)$ and of $[\mathrm{ACE}_i(z) - \mathrm{VAL}_i(z)]/\mathrm{MEAN}_i(z)$, the latter including some significant outliers. Histograms of the ACE-FTS and MLS N_2O VMRs, their differences, and their relative means were constructed at particular altitudes, and also confirmed this behaviour. In contrast, the relative deviation from the mean (solid blue line in Fig. 3c) is well behaved, with ACE-FTS agreeing to within ±7% from 15–50 km. Below 24 km, ACE-FTS has a high bias of +5 ppbv on average (10 ppbv maximum), with the relative deviation from the mean better than +3% on average (+5% maximum). Above 24 km, ACE-FTS has a low bias of −1 ppbv on average (−3 ppbv maximum), with the relative deviation from the mean better than −4% on average (−7% maximum). These results are consistent with Lambert et al. (2007), with the exception of the slightly larger relative deviation from the mean between 40 and 50 km.

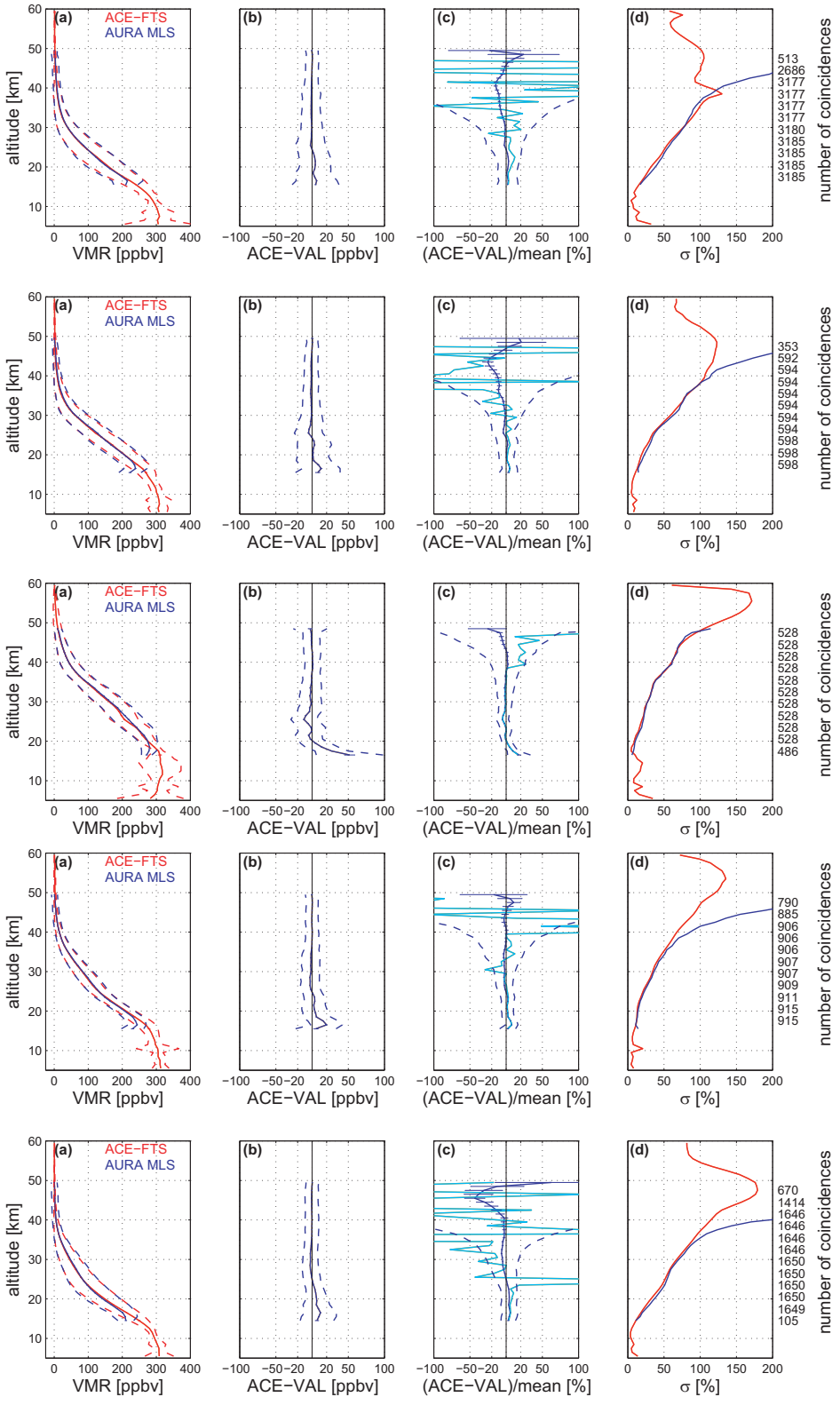

Fig. 4. Same as Fig. 2 but for comparisons between ACE-FTS and MLS. Top row: 60–90° N, second row: 30–60° N, third row: 30° S–30° N, fourth row: 30–60° S, bottom row: 60–90° S.

The latitudinal dependence of the ACE-FTS–MLS differences is seen in Fig. 4. In general the results are similar for the five bands, with mean absolute differences better than 10 ppbv between 15 and 50 km, and better than 5 ppbv above 20 km, with the exception of a few of the lowest altitudes seen in the tropics (30° S–30° N) and mid-latitudes (30°–60°). The ACE-FTS high bias (better than +10% relative deviation from the mean, except for the lowermost altitudes in the tropics) and low bias (except for the uppermost altitudes in the 30°–60° N and 60°–90° N) persist below and above 24 km, respectively.

4.3 MIPAS

The Michelson Interferometer for Passive Atmospheric Sounding (MIPAS) is an infrared limb-sounding Fourier transform interferometer on board Envisat, launched in March 2002 (Fischer et al., 2008). It acquires spectra over the range 685–2410 cm^{-1} (14.5–4.1 μm), which includes the vibration-rotation bands of many molecules of interest. It is capable of measuring continuously around an orbit in both day and night, and complete pole-to-pole coverage is obtained in 24 h. From 6 July 2002 until 26 March 2004, MIPAS was operated at full spectral resolution (0.025 cm^{-1}) with a nominal limb-scanning sequence of 17 steps from 68–6 km with 3 km tangent height spacing in the troposphere and stratosphere, generating complete profiles spaced approximately every 500 km along the orbit. However, in March 2004 operations were suspended following problems with the interferometer slide mechanism. Operations were resumed in January 2005 with a 35% duty cycle and reduced spectral resolution (0.0625 cm^{-1}). In this section, we describe comparisons between ACE-FTS and MIPAS N_2O products from the full-resolution mission generated by the ESA operational processor version 4.62 (hereafter referred to as MIPAS ESA) and by the Institut für Meteorologie und Klimaforschung (IMK)/Instituto de Astrofísica de Andalucía (IAA) scientific processor version 9 (hereafter referred to as MIPAS IMK-IAA). Negative values in the ESA data product are set to zero; at altitudes above ∼40 km, where the N_2O VMR is very small, this can result in a high bias of ESA N_2O relative to IMK-IAA N_2O.

4.3.1 MIPAS ESA N_2O

For the high-resolution mission, ESA has processed pressure, temperature, and six species (H_2O, O_3, HNO_3, CH_4, N_2O and NO_2). The algorithm used for the level 2 analysis is based on the Optimised Retrieval Model (ORM) (Raspollini et al., 2006; Ridolfi et al., 2000) and uses microwindows at 1233.275–1236.275 cm^{-1} and 1272.05–1275.05 cm^{-1} for the N_2O retrievals. MIPAS-ESA retrievals use the MIPAS dedicated spectroscopic database (see Raspollini et al. (2006) and references therein). Here, MIPAS v4.62 N_2O data are compared with ACE-FTS version 2.2 data from 21 February 2004 to 26 March 2004, when the MIPAS full-resolution mode data ended. The vertical resolution of the MIPAS VMR profiles is 3–4 km and the horizontal resolution is 300–500 km along-track (Fischer et al., 2008). During the first five months of ACE science operations, only sunsets were measured because of problems with spacecraft pointing at sunrise. Therefore the latitude coverage for this comparison is limited to 20° N–85° N for the selected coincidence criteria of ±6 h and 300 km. The intercomparison has been done including all the matching pairs of measurements available in the test period, which yields 141 coincidences (with single counting of profiles). For both ACE-FTS and MIPAS ESA, only profiles associated with successful pressure, temperature and target species retrievals have been considered.

As far as MIPAS ESA errors are concerned, we refer, in general, to the ESA level 2 products for the random error due to propagation of the instrument noise through the retrieval (see Piccolo and Dudhia (2007)), and to results of the analysis carried out at University of Oxford (see data available at http://www-atm.physics.ox.ac.uk/group/mipas/err) for the systematic error. Some of the components, listed in the Oxford University data set as systematic error on the individual profiles, show a random variability over the longer time-scales involved when averaging different MIPAS scans and/or orbits and tend to contribute to the standard deviation of the mean difference rather than to the bias. Taking this into account, for this intercomparison with ACE-FTS, we have considered the error contribution due to propagation of pressure and temperature random covariance into the retrieval of key species VMR (taken from the Oxford University data set) as a randomly variable component and combined it with the measurement noise – using the root-sum-square method – to obtain MIPAS ESA random error. For the MIPAS ESA profiles used in this work, the random error is less than 20% between 15 and 28 km, increasing to 75% at 6 km and to more than 80% above 36 km.

Figure 5 shows the results of the comparison. The mean absolute difference is as large as −38 ppbv at 6.5 km, within ±17 ppbv from 8–60 km, within ±10 ppbv above 15 km, with typical values of ±2 ppbv, particularly above 20 km. ACE-FTS has a low bias relative to MIPAS ESA between 6–10 km, 15–20 km, and 32–60 km. For this comparison, the mean relative difference and the relative deviation from the mean are similar and within ±10% (±4 typical) from 8 to 26 km, then increasing steadily to values greater than −20% in the relative deviation from the mean above 35 km, where the standard deviations on the mean ACE-FTS and MIPAS profiles are also large. The pronounced low bias of ACE-FTS compared to MIPAS ESA at higher altitudes is probably due to the negative values in the ESA data product being set to zero.

4.3.2 MIPAS IMK-IAA N_2O

The strategy and characteristics of the MIPAS IMK-IAA N_2O vertical profile retrievals are described by Glatthor et

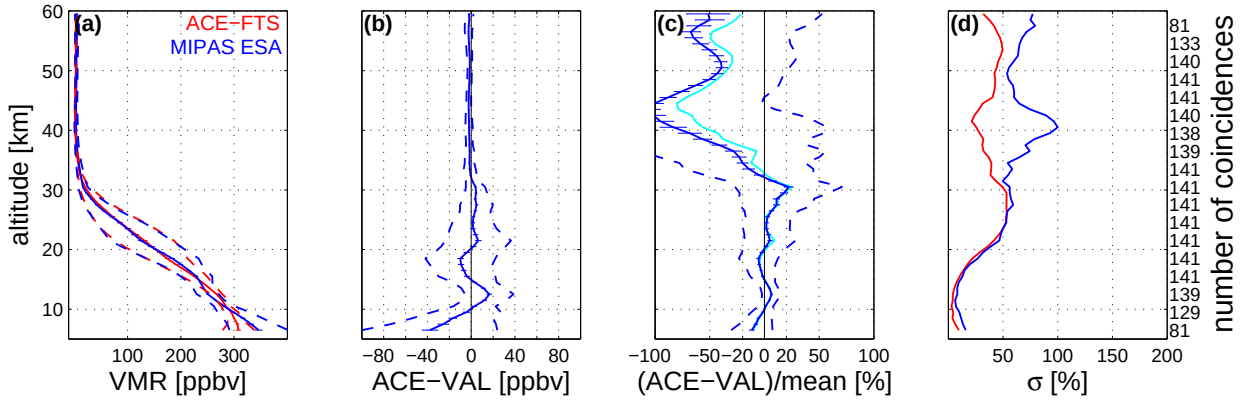

Fig. 5. Same as Fig. 1 but for comparisons between ACE-FTS and the MIPAS ESA N_2O data product from 20–85° N.

al. (2005). N_2O is retrieved jointly with CH_4 from its infrared emission lines in the spectral range from 1230 to 1305 cm^{-1}. Spectroscopic data are taken from the HITRAN 2004 database (Rothman et al., 2005). The vertical resolution in the case of mid-latitude profiles is about 3–4 km up to altitudes around 40 km, and increases to 6 km at an altitude of 50 km. The noise error is less than or equal to 5% up to 50 km. The systematic errors are within 12% up to 30 km and increase up to 33% above 30 km (Glatthor et al., 2005). The latter include the spectroscopic contribution, because although both MIPAS IMK-IAA and ACE-FTS retrieve N_2O using spectral microwindows near 1200 cm^{-1}, ACE-FTS also uses a series of microwindows between 1860 and 2600 cm^{-1}. It is possible that those bands will have different spectroscopic errors, which will not cancel totally even when using the same version of the HITRAN database.

Here we compare N_2O profiles from ACE-FTS sunset observations with MIPAS IMK-IAA measurements from 21 February 2004 until 25 March 2004. For these comparisons, we used as coincidence criteria a maximum time difference of 9 h, a maximum tangent point difference of 800 km, and a maximum potential vorticity (PV) difference of 3×10^{-6} $km^2\,kg^{-1}\,s^{-1}$ on the 475 K potential temperature level. Over all matches, this resulted in a mean distance of 296 km (±154 km), a mean PV difference of -0.007×10^{-6} $km^2\,kg^{-1}\,s^{-1}$ ($\pm1.49\times10^{-6}$ $km^2\,kg^{-1}\,s^{-1}$) and a mean time difference of −0.2 h. The distribution of the time differences is bi-modal since MIPAS measurements are either at around late morning or early night, while the ACE-FTS observations used here are made during sunset. Thus, for nighttime MIPAS observations, the time difference (MIPAS–ACE) is 4–5 h, while in the case of MIPAS daytime measurements it is about −6 to −8 h. Since N_2O shows no diurnal cycle in the sounded altitude range and since there is no significant difference between the daytime and nighttime comparisons, in the following we show the mean differences for day- and night-time matches together, as was done for the comparisons with the MIPAS ESA product.

Nevertheless, stratospheric N_2O profiles are affected by the subsidence inside the Arctic polar vortex. Thus, in Fig. 6 we show separately the results of the comparisons outside (372 coincidences with single counting of profiles) and inside (114 coincidences) the polar vortex. We determined the matches outside (inside) the vortex by values of PV of $<30\times10^{-6}$ ($>35\times10^{-6}$) $km^2\,kg^{-1}\,s^{-1}$ on the 475 K potential temperature level. Both instruments nicely detect the typical subsidence of inner vortex N_2O profiles compared to extra-vortex measurements. In general, the differences between MIPAS and ACE-FTS are similar irrespective of their position relative to the vortex. Over the entire 11–60 km altitude range of the comparison, the mean absolute differences are typically −3 ppbv (maximum difference −30 ppbv) inside the vortex and −5 ppbv (maximum difference −42 ppbv) outside. The corresponding relative deviations from the mean are typically −6% (maximum −43%) inside the vortex, and +3% (maximum +48%) outside, with oscillations about 0 as seen in Fig. 6c. Below about 26 km, ACE-FTS is smaller than MIPAS both outside and inside the vortex. The absolute differences are largest below about 18 km, which can be attributed to a high bias in the MIPAS data that has also been observed in other comparisons. However, the reason for the bump (+20%) at 30 km in the extra-vortex observations is an open issue. The relative deviations from the mean are largest at the highest altitudes, as expected given the very small N_2O VMRs in that region. The best agreement between ACE-FTS and MIPAS, taking into account both the mean absolute differences and the relative deviations from the mean, is seen between 18 and 35 km. In this region, on average, the mean absolute differences are −1 ppbv (−6 ppbv maximum) and −3 ppbv (−14 ppbv maximum) inside and outside the vortex, respectively, while the

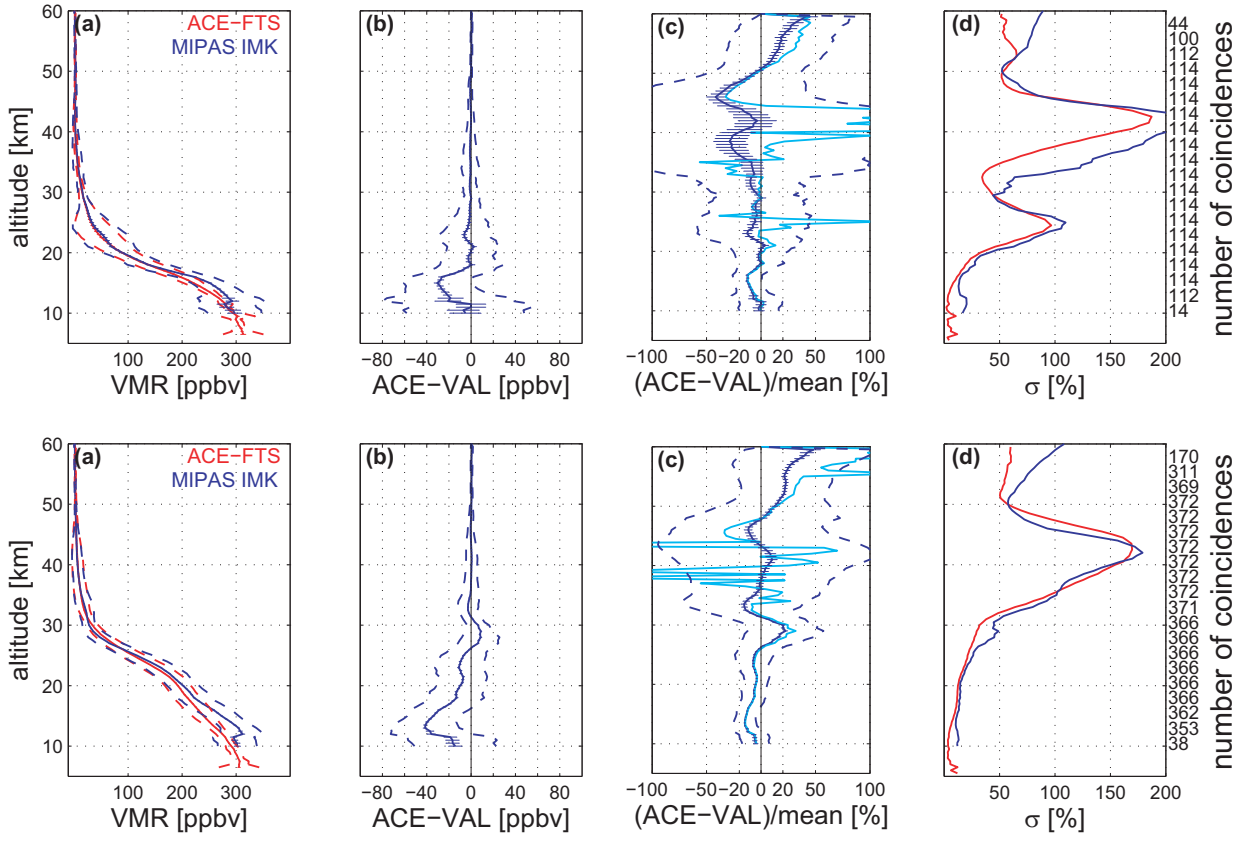

Fig. 6. Same as Fig. 1 but for comparisons between ACE-FTS and the MIPAS IMK-IAA N_2O data product for coincident measurements from 30–90° N inside (top row) and outside (bottom row) the polar vortex.

corresponding relative deviations from the mean are −5% (−13% maximum) and −1% (+22% maximum) inside and outside, respectively. It is also interesting to note the very similar variability observed by ACE-FTS and MIPAS, as seen in the standard deviations in Fig. 6d.

5 Comparisons with aircraft and balloon-borne measurements

5.1 ASUR

The Airborne Submillimeter wave Radiometer from the University of Bremen is a passive heterodyne radiometer operating in the frequency range from 604.3 to 662.3 GHz (von Koenig et al., 2000), which measures a number of species, including N_2O, O_3, HNO_3, and CO. Stratospheric N_2O measurements obtained with the Acousto Optical Spectrometer are used in this study. The total bandwidth of the spectrometer is 1.5 GHz and its resolution is 1.27 MHz; N_2O is retrieved using the 652.833 GHz line. This receiver is designed to carry out measurements from a high-altitude research aircraft in order to avoid signal absorption by tropospheric water vapor during the observations. ASUR is an upward-looking instrument at a stabilized constant zenith angle of 78°. The receiver measures thermal emissions from the rotational lines of the target molecule. The shape of the pressure-broadened lines is related to the vertical distribution of the trace gas. The measured spectra are integrated up to 150 s, which leads to a horizontal resolution of about 30 km along the flight path. The vertical profiles of the molecule are retrieved on an equidistant altitude grid of 2-km spacing using the optimal estimation method (Rodgers, 2000). The vertical resolution of the N_2O measurements is 8–16 km and the vertical range is 18 to 46 km. The precision of a typical single measurement is 10 ppbv and the accuracy is 15% or 30 ppbv, whichever is larger, including systematic uncertainties. Details about the measurement technique and retrieval theory can be found in Kuttippurath (2005).

The ASUR N_2O measurements used here were performed during the Polar Aura Validation Experiment (PAVE) campaign (http://www.espo.nasa.gov/ave-polar/). Data from five selected ASUR measurement flights (on 24, 25, and 31 January 2005, and 2 and 7 February 2005) during the campaign are compared with ACE-FTS occultations between 60° N and 70° N. ASUR measurements within 1000 km and ±12 h of the satellite observations were selected, yielding seven

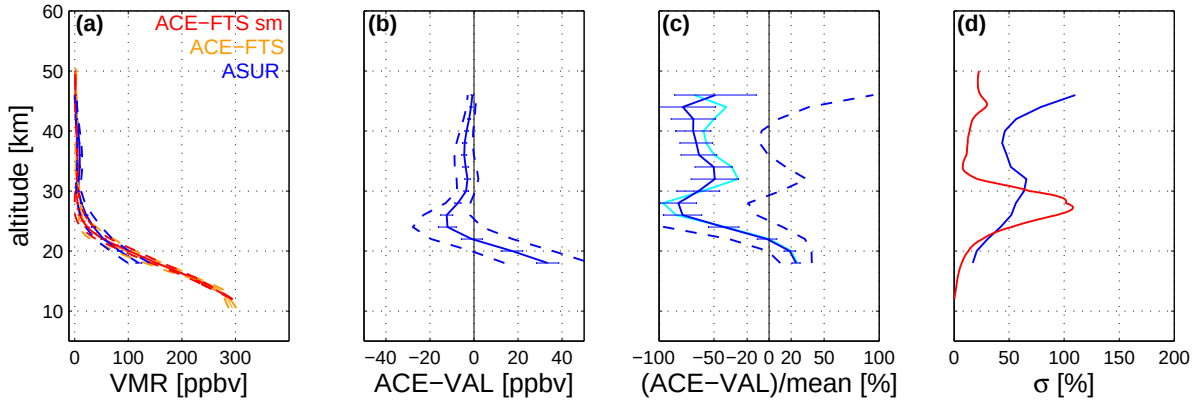

Fig. 7. Same as Fig. 1 for comparisons between ACE-FTS and ASUR, except that in panel **(a)** the original ACE-FTS profile is now plotted in orange and the ACE-FTS profile smoothed by the ASUR averaging kernels is plotted in red. The smoothed ACE-FTS profile is used for the results shown in panels **(b)**, **(c)**, and **(d)**. The latitude range for the comparisons is 60–70° N.

ACE-FTS profiles, 15 ASUR profiles, and 17 co-located observation pairs. Because the vertical resolution of the ASUR profiles is lower than that of the satellite profiles, the ACE-FTS N_2O vertical profiles were convolved with the ASUR N_2O averaging kernels, and compared on the 2-km ASUR altitude grid.

Figure 7 shows the results from the comparison. The best agreement between the ASUR and ACE-FTS mean absolute difference profiles is between 30 and 46 km, where they agree to within −4.5 ppbv and on average, to within −3 ppbv. Between 18 and 30 km, the maximum difference is +33 ppbv and typical differences are within ±10 ppbv. The ACE-FTS profiles are consistently smaller than ASUR above 22 km, and larger for the comparisons at 18 and 20 km. The relative deviations from the mean are large, reaching a maximum of +82% at 28 km. In general, the ACE-FTS profiles are in reasonable agreement with the ASUR profiles, as the differences are well within the estimated accuracy of ASUR N_2O, i.e., 30 ppbv.

5.2 SPIRALE

SPIRALE (Spectroscopie Infra-Rouge d'Absorption par Lasers Embarqués) is a balloon-borne tunable diode laser absorption spectrometer operated by LPCE (Laboratoire de Physique et Chimie de L'Environment, CNRS-Université d'Orléans) (Moreau et al., 2005), which has participated in several European satellite validation campaigns for Odin and Envisat. It can perform simultaneous in situ measurements of about ten chemical species from about 10 to 35 km height, with a high-frequency sampling (∼1 Hz), thus enabling a vertical resolution of a few meters depending on the ascent rate of the balloon. It has six tunable diode lasers that emit in the mid-infrared from 3 to 8 μm, with beams injected into a multi-pass Heriott cell located under the gondola and largely exposed to ambient air. The 3.5-m-long cell is deployed during the ascent when the pressure is less than 300 hPa, and provides a total optical path between the two cell mirrors of 430.78 m. N_2O concentrations are retrieved from direct infrared absorption of the ro-vibrational line at 1275.49 cm^{-1}, by fitting experimental spectra with spectra calculated using the HITRAN 2004 database (Rothman et al., 2005). Measurements of pressure (by two calibrated and temperature-regulated capacitance manometers) and temperature (by two probes made of resistive platinum wire) aboard the gondola allow conversion of the measured number densities into VMRs. Uncertainties on these parameters and on the spectroscopic data (essentially molecular line strength and pressure broadening coefficients) are negligible relative to the other sources of error. The uncertainties in the VMRs have been assessed by taking into account random and systematic errors, and combining them as the square root of their quadratic sum. The random errors (fluctuations of the laser background emission signal and signal-to-noise ratio) and the systematic errors (laser line width and non-linearity of the detector) are very low, resulting in an estimated total uncertainty of 3% for N_2O volume mixing ratios above 3 ppbv (i.e., at altitudes <26 km) and 6% for mixing ratios below 3 ppbv (>26 km).

The SPIRALE balloon flight occurred on 20 January 2006 between 17:46 UT and 19:47 UT, with a vertical profile obtained during ascent between 13.2 and 27.2 km. The measurement position remained rather constant, with the balloon mean location at 67.6±0.2° N and 21.55±0.20° E. The comparison is made with ACE-FTS sunrise occultation sr13151, which occurred 13 hours later (on 21 January 2006 at 08:00 UT) and located at 64.28° N and 21.56° E, i.e., 413 km away from SPIRALE. Using the MIMOSA (Modélisation Isentrope du transport Méso-échelle de l'Ozone Stratosphérique par Advection) contour advection model (Hauchecorne et al., 2002), PV maps in the region of both measurements have been calculated each hour between 17:00 UT on 20 January and 08:00 UT on 21 January on isentropic surfaces, every 50 K from 350 K to 800 K

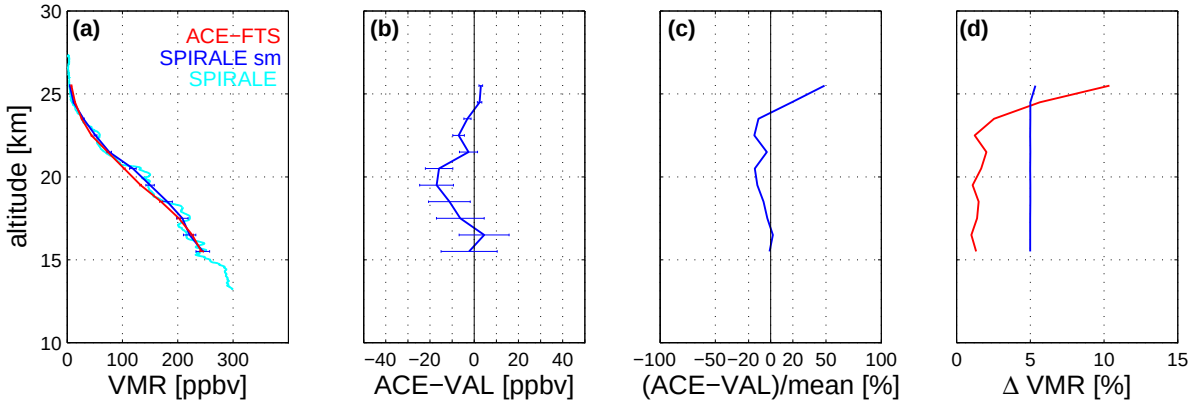

Fig. 8. (a) Single N_2O vertical profiles obtained by SPIRALE on 20 January 2006 and during ACE-FTS occultation sr13151 (red). The cyan line corresponds to the original SPIRALE measurements and the blue line corresponds to the SPIRALE profile smoothed with a triangular function (see text). Uncertainties are shown as error bars on both profiles. **(b)** Absolute difference profile (solid line) with error bars representing the combined random error, computed as the root-sum-square error of the ACE-FTS fitting error and the SPIRALE uncertainty. **(c)** Relative difference profile, as a percentage of the mean profile. **(d)** The fractional values of the ACE-FTS fitting error (red) and the SPIRALE uncertainty (blue) as percentages.

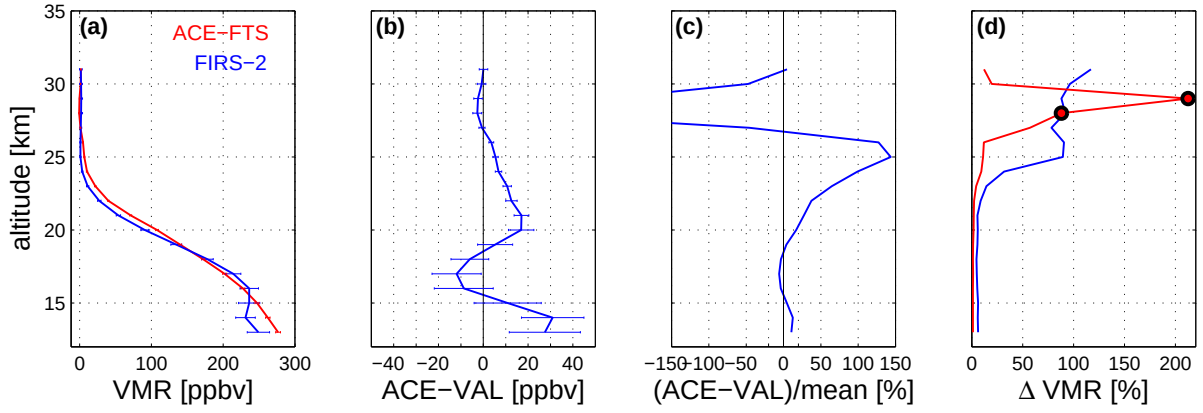

Fig. 9. Same as Fig. 8, but for the FIRS-2 balloon flight of 24 January 2007 and ACE occultation sr18561. The two points marked in panel **(d)** are altitudes (28 and 29 km) for which the ACE-FTS N_2O VMR is negative and so these fractional uncertainty values are also negative. However, the absolute values have been plotted here to allow a reasonable x-axis scale.

(corresponding to 12.8–30 km height). These PV fields indicated that SPIRALE and ACE-FTS sampled similar air masses within the polar vortex, with PV agreement better than 10%.

Given the very high vertical resolution (on the order of meters) of the SPIRALE N_2O profile, it was smoothed by a set of triangular weighting functions of 3 km at the base and interpolated onto the ACE-FTS 1-km grid as discussed in Sect. 3. This smoothing truncated the bottom and the top of the SPIRALE profile by 1.5 km. Figure 8 shows that the ACE-FTS and SPIRALE N_2O profiles agree to within 17 ppbv (and are typically within ±6 ppbv) in the 15 to 26 km altitude range, with relative differences between −15% and +19% (and ±5% on average) except at the highest altitude, where the difference increases to +49%. ACE-FTS is consistently smaller than SPIRALE between 17 and 24 km.

5.3 FIRS-2

FIRS-2 (Far-InfraRed Spectrometer-2) is a balloon-borne Fourier transform infrared spectrometer designed and built at the Smithsonian Astrophysical Observatory. It has contributed to numerous previous satellite validation efforts (e.g., Roche et al., 1996; Jucks et al., 2002; Nakajima et al., 2002; Canty et al., 2006). FIRS-2 detects atmospheric thermal emission in limb-viewing mode from approximately 7 to 120 μm at a spectral resolution of 0.004 cm^{-1} (Johnson et al., 1995). Vertical profiles of about 30 trace gases are retrieved from the float altitude (typically 38 km) down to the tropopause using a nonlinear Levenberg-Marquardt least-squares algorithm, with pressure and temperature profiles derived from the 15 μm band of CO_2. Uncertainty estimates for FIRS-2 contain random retrieval error from spectral noise

Table 2. The ground-based FTIR stations contributing N_2O partial columns for comparisons with ACE-FTS. The location (latitude, longitude, and altitude in m above sea level, a.s.l.) of each station is listed, along with the instrument manufacturer and model, the nominal spectral resolution for the measurements used in this study, the retrieval code and microwindows (MW) used to derive N_2O partial columns, and references that provide additional details regarding the stations and their measurements. Where multiple MWs are listed, these were fitted simultaneously to retrieve N_2O.

Station	Location	Alt. (m a.s.l.)	Instrument	Res'n (cm^{-1})	Retrieval Code	N_2O MW (cm^{-1})	Reference
Ny-Ålesund	78.9° N, 11.9° E	20	Bruker 120HR	0.004	SFIT2 3.92a	2481.3–2482.6	Notholt et al. (1997)
Thule	76.5° N, 68.7° W	225	Bruker 120M	0.004	SFIT2 3.92b	2484.4–2485.9	Goldman et al. (1999)
Kiruna	67.8° N, 20.4° E	419	Bruker 120HR	0.005	PROFFIT92	2481.3–2482.6 2526.4–2528.2 2537.85–2538.8 2540.1–2540.7	Blumenstock et al. (2006)
Harestua	60.2° N, 10.8° E	596	Bruker 120M	0.005	SFIT2 3.81	2481.28–2482.62 2526.4–2528.2 2537.84–2538.82 2540.00–2540.75	Paton-Walsh et al. (1997)
Bremen	53.1° N, 8.9° E	27	Bruker 125HR	0.004	SFIT2 3.92a	2481.3–2482.6	Buchwitz et al. (2007)
Jungfraujoch	46.5° N, 8.0° E	3580	Bruker 120HR	0.005 or 0.003	SFIT2 3.91	2481.3–2482.6 2526.4–2528.2 2537.85–2538.8 2540.1–2540.7	Mahieu et al. (1997) Zander et al. (2008)
Toronto	43.7° N, 79.4° W	174	Bomem DA8	0.004	SFIT2 3.82B3	2481.3–2482.6	Wiacek et al. (2007)
Izaña	28.3° N, 16.5 ° W	2367	Bruker 120M (to December 2004) Bruker 125HR (since Jan. 2005)	0.005	PROFFIT92	2481.3–2482.6 2526.4–2528.2 2537.85–2538.8 2540.1–2540.7	Schneider et al. (2005)
Reunion Island	20.9° S, 55.5° E	50	Bruker 120M	0.005	SFIT2 3.92	2481.3–482.6 2526.4–2528.2 2537.85–2538.8 2540.1–2540.7	Senten et al. (2008)
Wollongong	34.5° S, 150.9° E	30	Bomem DA8	0.004	SFIT2 3.92	2481.2–2482.0 2482.0–2482.8 2482.8–2483.5	Paton-Walsh et al. (2005)
Lauder	45.0° S, 169.7° E	370	Bruker 120HR	0.0035	SFIT2 3.82	2481.2–2483.5	Griffith et al. (2003)
Arrival Heights	77.8° S, 166.6° E	200	Bruker 120M	0.0035	SFIT2 3.82	2481.2–2483.5	Wood et al. (2002)

and systematic components from errors in atmospheric temperature and pointing angle (Johnson et al., 1995; Jucks et al., 2002). N_2O profiles are retrieved using the ν_2 band between 550 and 600 cm^{-1}.

ACE-FTS is compared with the N_2O profile obtained during a FIRS-2 balloon flight from Esrange, Sweden on 24 January 2007. The average location of the flight was 67.27° N, 27.29° E, with some smearing of the longitude footprint as FIRS-2 was observing to the east. The data were recorded before local solar noon, at 10:11 UT, with a solar zenith angle of 86.6°. The float altitude was just under 28 km, limiting the maximum measurement altitude to 31 km. The 1σ error on the measured N_2O VMR varied from 5–14% between 13 and 23 km, and increased steadily above 23 km to 117% at 31 km. The closest ACE-FTS occultation was sr18561, obtained on 23 January 2007, at 08:25 UT, 64.70° N, 15.02° E, placing it 481 km away from the location of the balloon flight, and almost 26 h earlier. The FIRS-2 footprint was inside the vortex,

Table 3. Summary of the results of the N_2O partial column comparisons between ACE-FTS and the ground-based FTIR stations. N is the number of coincidences, Δd and Δt are the mean distance and time, respectively, between ACE-FTS occultations and the FTIR stations, along with the corresponding standard deviations, Δz is the partial column altitude range, and DOFS is the degrees of freedom for signal for the FTIR partial columns over the given altitude range of the comparison. The mean relative difference is calculated as 100% × the mean of the N differences (ACE-FTS–FTIR)/FTIR, and is given along with the standard error on the mean, and the standard deviation on the ensemble. For Harestua, Kiruna, and Izaña, the mean relative differences given in brackets are corrected for the 1.3% bias due to the use of HITRAN 2000.

Station	N	Δd (km) ± std. devn. (km)	Δt (h) ± std. devn. (h)	Δz (km)	DOFS (FTIR)	Relative diff. (%) ± std. error (%)	Std. devn. (%)
Ny-Ålesund	15	722±118	5.1±3	11.2–24.4	1.5	3.8±0.6	2.4
Thule	29	633±246	6±4	8.6–29.0	1.0	−0.8±1.6	8.6
Kiruna	18	317±145	6.1±3.9	15.9–29.1	1.1	−6.6 (−5.3) ±5.2	22.1
Harestua	24	703±180	12.4±6	15.1–29.1	1.8	−18.6 (−17.3) ±6.0	29.6
Bremen	39	606±244	11.9±5.2	13.6–22.0	0.7	−0.6±0.6	3.9
Jungfraujoch	24	647±247	7.7±5.1	16.0–29.2	1.6	−0.4±1.1	5.6
Toronto	31	591±205	11±6.2	17.0–28.9	1.8	−5.5±1.3	7.3
Izaña	10	707±139	16.1±5.6	16.0–24.8	1.1	−0.2 (1.1)±3.4	10.8
Reunion Island	5	1004±168	14.4±7.2	16.0–24.4	0.9	−5.6±4.8	10.8
Wollongong	7	940±230	8.8±6.8	15.0–29.0	1.4	−3.9±1.6	4.2
Lauder	35	702±231	11.2±6.7	15.0–27.0	1.5	−3.9±1.0	6.2
Arrival Heights	18	612±240	10.1±5.8	13.0–27.0	1.7	1.9±4.2	17.8

while the ACE-FTS occultation was nearer the vortex edge. The FIRS-2 N_2O profile, reported on a 1-km grid, was interpolated onto the ACE-FTS 1-km grid.

Figure 9 shows the results of the comparison. The absolute differences vary from −12 to +30 ppbv over the full altitude range of 13–31 km, with typical values of of +8 and +5 ppbv below and above 20 km, respectively. The largest absolute differences are below 15 km, where FIRS-2 reported low values of N_2O, although the relative differences have maxima at 25 and 28 km (>±100%). It is possible that FIRS-2 is seeing subsidence within the vortex. Below 20 km, the relative differences are between −6% and +17%, but they increase significantly above 20 km. ACE-FTS has a low bias relative to FIRS-2 between 11 and 13 km, and between 27 and 30 km.

6 Comparisons with ground-based FTIR measurements

In addition to the vertical profile comparisons described above, ACE-FTS N_2O measurements have been compared with partial columns retrieved from solar absorption spectra recorded by ground-based Fourier transform infrared spectrometers. Twelve such instruments participated in this study; all are at stations of the Network for the Detection of Atmospheric Composition Change (NDACC) (Kurylo and Zander, 2000) and make regular measurements of a suite of tropospheric and stratospheric species. Many have previously provided data for validation of N_2O measurements by satellite instruments, such as ILAS (Wood et al., 2002), ILAS-II (Griesfeller et al., 2006), SCIAMACHY (Dils et al., 2006), and MIPAS (Vigouroux et al., 2007). Table 2 lists the stations involved, including their location, the instrument type and spectral resolution, and the retrieval code and microwindows used to retrieve N_2O. More information about the instruments, the retrieval methodologies, and the measurements made at each of these sites can be found in the references provided in Table 2. The participating stations cover latitudes from 77.8° S to 78.9° N, and provide measurements from the subtropics to the polar regions in both hemispheres.

The FTIR measurements require clear-sky conditions, but are made year-round, thus providing good temporal coverage for comparisons with ACE-FTS. The data used here were analyzed using either the SFIT2 retrieval code (Pougatchev and Rinsland, 1995; Pougatchev et al., 1995; Rinsland et al., 1998) or PROFFIT92 (Hase, 2000). Hase et al. (2004) found that N_2O VMR profiles retrieved using these two codes showed very good agreement, with total columns agreeing to within 1%. Both algorithms employ the optimal estimation method (Rodgers, 2000) to retrieve vertical profiles from a statistical weighting between a priori information and the high-resolution spectral measurements. Barbe and Marche (1985) and Sussmann and Schäfer (1997) also showed how information on the vertical distribution of N_2O could be derived from ground-based infrared spectra. Averaging kernels calculated as part of the optimal estimation analysis quantify the information content of the retrievals, and can be convolved with the ACE-FTS profiles, which have higher vertical resolution. For N_2O, there are typically 3–4 Degrees Of Freedom for Signal (DOFS, equal to the trace of the averaging kernel matrix) in the total column, and 1–2 in the altitude

range coincident with ACE-FTS measurements. Given this coarse vertical resolution, we compare partial columns rather than profiles. All participating sites used microwindows in the 2480–2485 cm^{-1} region for the N_2O retrievals, with several sites also including microwindows between 2526 and 2541 cm^{-1}; these are listed in Table 2. All sites used spectroscopic data from HITRAN 2004, with the exception of Harestua, which used HITRAN 2000, and Kiruna and Izaña, which used HITRAN 2000 + official updates (equivalent to HITRAN 2000 for N_2O). Recent analysis using Kiruna data coincident with ACE-FTS has shown that N_2O columns retrieved with HITRAN 2000 are 1.3% larger than those retrieved with HITRAN 2004. This means that the Harestua, Kiruna, and Izaña retrieved N_2O columns will be biased positive, so that the ACE-FTS – FTIR differences will be biased slightly negative. Other information required for the retrievals, such as a priori profiles and covariances, treatment of instrument lineshape, and atmospheric temperature and pressure are optimized for each site as appropriate for the local conditions.

The coincidence criteria applied for the FTIR comparisons were ±24 h and 1000 km, with two exceptions. For Kiruna, tighter criteria of ±12 h and 500 km were used in order to minimize the potential influence of the polar vortex, and for Reunion Island, the criteria were ±24 h, ±15° longitude, and ±10° latitude, resulting in a maximum distance of 1211 km. These relatively relaxed criteria were necessary to obtain a reasonable number of ACE overpasses for each station (between 5 and 39), and are generally used in FTIR-satellite comparisons, particularly for a well-mixed, long-lived species such as N_2O. In cases where several ACE occultations met the coincidence criterion for one FTIR measurement at a site, only the occultation that was closest (optimized for the combination of temporal and spatial coincidence) was used. For each FTIR station, the mean (and standard deviation) distance and time differences for these closest ACE occultations are listed in Table 3. Overall, considering all coincident pairs of ACE-FTS and FTIR measurements, the mean distance is 637±253 km and the mean time difference (calculating all time differences as positive) is 9.9±6.2 h. Coincidences from February 2004 through December 2006 were included in the comparisons.

For each station, the ACE-FTS profiles were interpolated onto the FTIR retrieval grid and extended below the lowest retrieved altitude using the FTIR a priori VMR values. This combined profile was smoothed using the FTIR averaging kernels and a priori profile, as described in Sect. 3, to minimize the smoothing error (Rodgers and Connor, 2003). For the calculation of partial columns, atmospheric densities were needed; the density derived from the pressure and temperature profiles used in the FTIR retrievals was used for both the ACE-FTS and ground-based measurements. The lower limit of the altitude range of the partial columns at each station was determined by the ACE-FTS altitudes and the upper limit was determined by the sensitivity of the FTIR measurements, defined for a given altitude as the sum of the elements of the corresponding averaging kernel (Vigouroux et al., 2007). This sensitivity was required to be 0.5 or greater, indicating that the measurement contributes at least 50% to the retrieved profile, with the remainder coming from the a priori information (Vigouroux et al., 2007). As seen in Table 3, the lower limits ranged between 8.6 and 17.0 km, while the upper limits ranged between 22.0 and 29.2 km, and the corresponding DOFS for the partial columns varied from 0.7 to 1.8. Over these altitude ranges, the uncertainty on the N_2O partial columns is on the order of 3% (calculated for the Toronto FTIR data), taking into account the measurement noise error (based on the root-mean-square of the noise in the spectrum and assumed to be uncorrelated so as to eliminate numerical ill-conditioning), the state space interference error (due to unphysical correlations between different parameters in the state space), and the temperature error (Rodgers and Connor, 2003).

The time series of the partial column comparisons are shown for all stations in Fig. 10, along with the relative differences as a percentage of the FTIR partial columns. Agreement is good: within ±20% for all but a few cases, and generally better than this. Table 3 summarizes these results, listing the mean relative differences (calculated as 100% × the mean of the N differences (ACE-FTS–FTIR)/FTIR), the standard errors on the mean, and the standard deviations. For Harestua, Kiruna, and Izaña, the values given in brackets are corrected for the 1.3% bias due to the use of HITRAN 2000, thus providing a consistent set of comparisons based on HITRAN 2004 spectroscopic data. The mean differences lie between (−18.6±6.0)% with $\sigma = 29.6\%$ for Harestua (−17.3% if adjusted to HITRAN 2004) and (+3.8±0.6)% with $\sigma = 2.4\%$ for Ny-Ålesund. There are some problems with oscillations in the N_2O profiles retrieved at Harestua, which may explain the difference in partial columns; this is currently under investigation. Examination of PV maps from the European Centre for Medium-range Weather Forecasts (not shown) suggests that the large relative differences seen in the Kiruna data between 25 January and 7 February 2005 are probably related to the polar vortex. With the exception of Harestua, all the mean relative differences are within ±5.6% (on the basis of HITRAN 2004 spectroscopic data). Given that the mean statistical fitting error for ACE-FTS N_2O is <4% between 5 and 35 km, and that the uncertainty on the FTIR N_2O partial columns is on the order of 3%, the mean relative differences are better than, or comparable to, the combined random error estimate of approximately 5%. These results are also consistent with those of Sung et al. (2007), who found that nine ACE-FTS N_2O partial columns (from 6 to 100 km) measured within 200 km of the PARIS-IR instrument at Eureka, Canada (80.05° N, 86.42° W) in spring 2004 agreed to within 5%. At ten of the twelve FTIR stations, the mean relative difference is negative, suggesting that the ACE-FTS partial columns have a small negative bias.

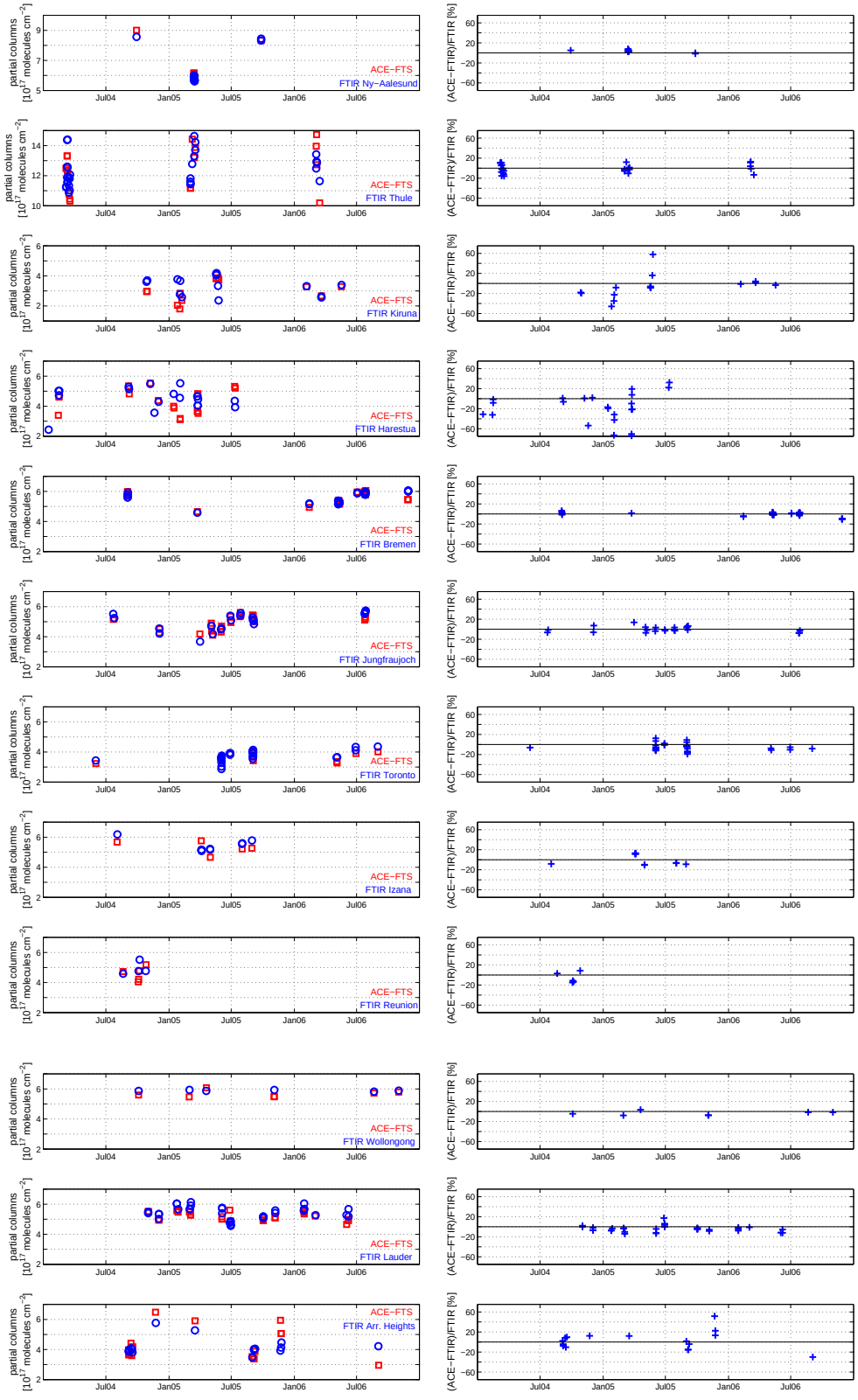

Fig. 10. Comparison of ACE-FTS and ground-based FTIR N_2O partial columns. For each station, the left-hand panel shows the time series of partial columns from ACE-FTS (red squares) and the FTIR (blue circles), and the right-hand panel shows the relative differences as a percentage of the FTIR partial columns. Note that the y-axis scales on the left-hand panels differ for some stations.

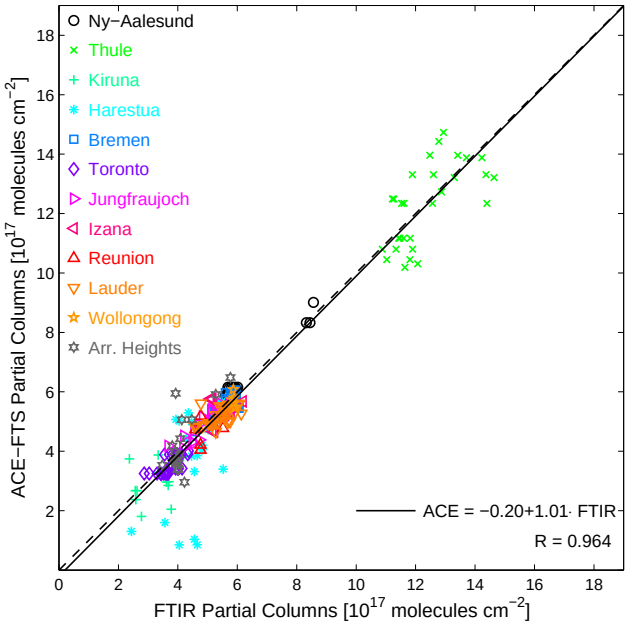

Fig. 11. Scatter plot of the ACE-FTS and ground-based FTIR N_2O partial columns shown in Fig. 10. The solid black line is the least-squares linear fit to the data, with the slope, intercept, and correlation coefficient given in the figure. The dotted line shows the one-to-one line relationship for comparison.

Excellent correlation between the ACE-FTS and FTIR partial columns is seen in the scatter plot of the complete data set. Figure 11 shows a tight correlation, with a correlation coefficient (R) of 0.964. The line fitted to the data has slope 1.01, indicating excellent agreement, and intercept −0.20, indicating a small systematic offset between the two datasets consistent with the small negative bias in ACE-FTS noted above. As might be expected, the largest standard deviations in Table 3 and the largest scatter in Fig. 11 are found for the high-latitude stations which may be viewing different airmasses from ACE and seeing (or not) subsidence within the polar vortex.

7 Conclusions

In this study, we have undertaken an assessment of the quality of the ACE-FTS version 2.2 N_2O data prior to its public release. N_2O is one of the 14 baseline species for the ACE mission, and version 2.2 VMR profiles are retrieved from solar occultation measurements in 69 microwindows between 1120 and 2600 cm^{-1}. The N_2O retrievals extend from 5 to 60 km at a vertical resolution of about 3–4 km, and have a precision (1σ statistical fitting error) that is typically less than 5%. ACE-FTS N_2O profiles from the first three years of the mission have been compared with coincident measurements made by the SMR, MLS, and MIPAS satellite instruments, multiple aircraft flights of ASUR, and individual balloon flights of SPIRALE and FIRS-2. ACE-FTS N_2O partial columns have been compared with measurements by twelve globally distributed ground-based FTIRs. In Fig. 12, the mean absolute differences and the relative deviations from the mean for all of the statistical and individual vertical profile comparisons are shown together, while Table 4 provides a summary of the results of these comparisons.

Excellent agreement between ACE-FTS and SMR (Chalmers v2.1) is seen in the mean absolute differences, which are typically −2 ppbv in the global comparison for 15–50 km, with a maximum difference of −10 ppbv at 15 km. ACE-FTS has a low bias relative to SMR at nearly all altitudes up to 54 km, and a small high bias above this. The relative deviations from the mean are typically −4% between 15 and 40 km, with a maximum difference of −20% at 40 km, increasing to more than 100% above 40 km due to the small values of the mean N_2O VMR. Little latitudinal dependence is seen in the comparisons.

The comparison with MLS (version 2.2) provided the largest number of coincident profiles and also resulted in very good agreement between the datasets. A high bias in ACE-FTS is seen between 15 and 24 km, typically +5 ppbv, and varying between +2 and +10 ppbv. Over this altitude range, the relative deviation from the mean varies from +2% to +5%. From 24–50 km, ACE-FTS has a low bias of −1 ppbv on average, with the relative deviation from the mean between −7% and 0. There is also little latitudinal dependence in the ACE-FTS–MLS differences, with the mean absolute differences consistently better than 10 ppbv between 15 and 50 km, and better than 5 ppbv above 20 km, with the exception of a few points. The ACE-FTS high and low bias persists below and above 24 km, respectively, for all five latitude bands examined.

ACE-FTS was compared with MIPAS N_2O profiles generated by the ESA operational processor (version 4.62) and by the IMK-IAA scientific processor (version 9). Comparisons with the ESA product provide validation results to the lowest altitude in this study, extending down to 6 km. At the lowest altitudes, the mean absolute difference is as large as −38 ppbv at 6.5 km, changing to +17 ppbv at 12.5 km and decreasing above. Below 32 km, the mean absolute difference oscillates about 0, with a mean value of −1 ppbv and a standard deviation of 12 ppbv. The corresponding relative deviation from the mean is +3±8%, with values ranging from −12% to +22%. Above 32 km, there is a persistent low bias in the ACE-FTS data, with mean absolute differences of −2 to −1 ppbv, but relative deviations from the mean increasing to −105%.

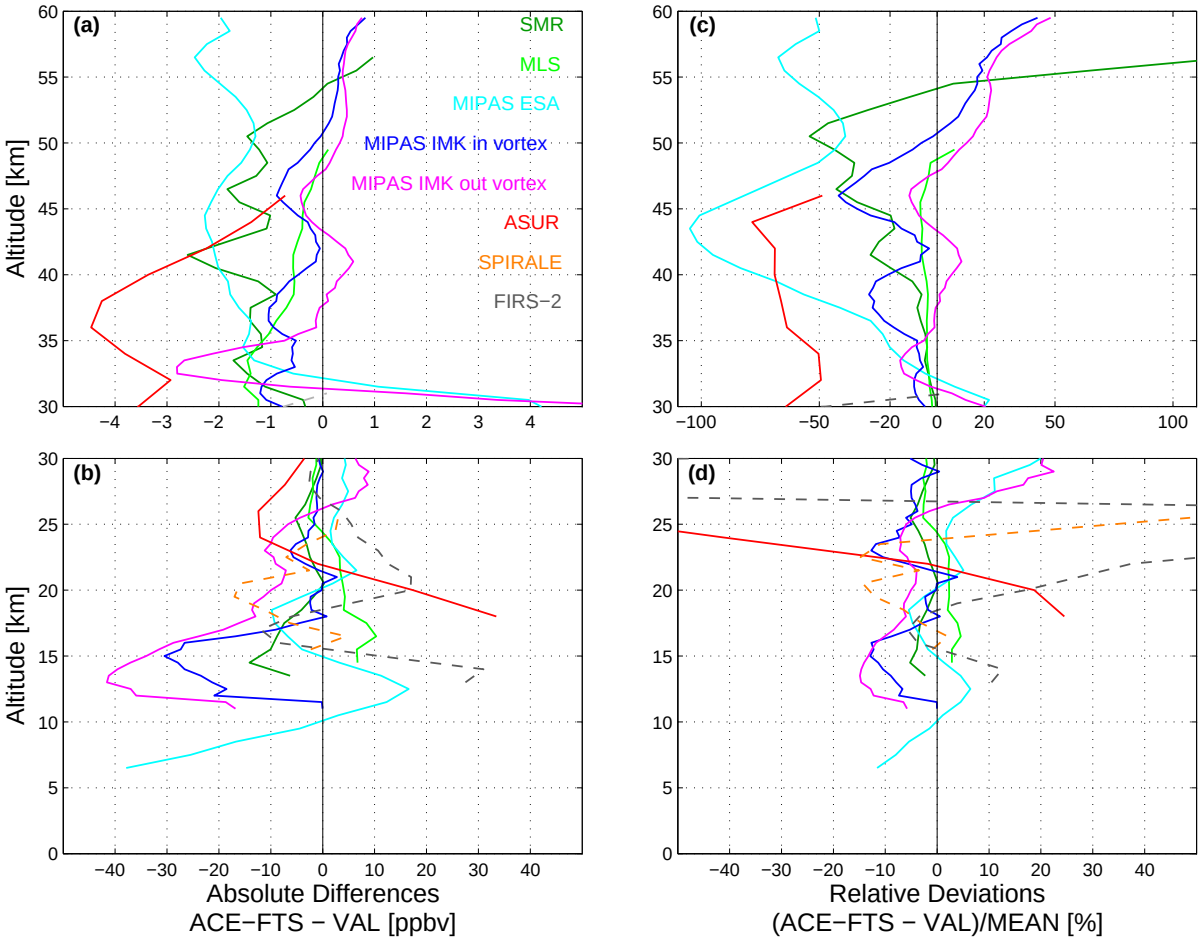

Fig. 12. Summary plots for all of the VMR profile comparisons for ACE-FTS N_2O. Profiles of the mean absolute differences **(a)** from 30 to 60 km, and **(b)** from 0 to 30 km. Profiles of the relative deviations from the mean **(c)** from 30 to 60 km, and **(d)** from 0 to 30 km. In both panels, the statistical comparisons are indicated by solid lines, and the individual profile comparisons are indicated by dashed lines.

The MIPAS IMK-IAA N_2O profiles extend from 11–60 km, over which range the mean absolute differences are typically −3 ppbv (maximum −30 ppbv) inside the vortex and −5 ppbv (maximum −42 ppbv) outside. The corresponding relative deviations from the mean are typically −6% (maximum −43%) inside the vortex, and +3% (maximum +48%) outside. The larger negative differences seen below 18 km can be attributed to the known high bias in MIPAS at those altitudes. The best agreement between ACE-FTS and MIPAS IMK-IAA N_2O is between 18 and 35 km, where the mean absolute differences are typically −1 ppbv (−6 to +3 ppbv) and −3 ppbv (−14 to +9 ppbv) inside and outside the vortex, respectively, while the corresponding relative deviations from the mean are −5% and −1%. The differences between the comparisons of ACE-FTS with the two MIPAS data products (ESA and IMK-IAA) can be partly explained by the suppression of negative values in the ESA N_2O VMRs, which leads, at altitudes above ∼40 km, to a high bias of ESA N_2O relative to IMK-IAA N_2O, and hence a more negative bias in the ACE-FTS–MIPAS ESA differences.

The fourth set of statistical comparisons involved 17 coincidences between ACE-FTS and ASUR aircraft observations. Between 18 and 30 km, the maximum mean absolute difference is +33 ppbv and typical differences are +2±17 ppbv, while from 30–46 km, the mean differences are better than −4 ppbv and on average, −3 ppbv. Although the relative deviations from the mean are large, the agreement between the ACE-FTS and ASUR profiles is generally well within the 30 ppbv accuracy of ASUR N_2O measurements.

Comparisons were also made with individual profiles obtained from two balloon flights. The ACE-FTS and SPIRALE profiles agree to within –17 ppbv (and within −5±7 on average) from 15 to 26 km, with relative differences within 19% except at the highest altitude (+49%). ACE-FTS has a low bias relative to SPIRALE between 17 and 24 km. Larger

Table 4. Summary of the results of the statistical and individual VMR profile comparisons for ACE-FTS N_2O. Note that absolute and relative differences for SPIRALE and FIRS-2 are for individual profile comparisons.

Instrument (retrieval code)	Number of coincidences	Altitude range (km)	Mean absolute differences (ppbv): mean $\pm1\sigma$	range (min. to max.)	Relative deviations from mean (%): mean $\pm1\sigma$	range (min. to max.)
SMR	1099	15–50	−2±1	−10 to 0	−11±15	−44 to 0
(Chalmers v2.1)		15–40	−3±3	−10 to 0	−4±4	−20 to 0
MLS	6876	15–24	+5 ±3	+2 to +10	+3±1	+2 to +5
(version 2.2)		24–50	−1±1	−3 to 0	−4±2	−7 to 0
MIPAS ESA	141	6–32	−1±12	−38 to +17	+3 ± 8	−12 to +22
(version 4.62)		32–60	−2 ± 0.4	−2 to −1	−57±27	−105 to −5
MIPAS IMK-IAA	114 inside vortex	11–60	−3±7	−30 to +3	−6±16	−42 to +43
(version 9)		18–35	−1±2	−6 to +3	−5±4	−13 to +4
	372 outside vortex	11–60	−5±12	−42 to +9	+3±15	−16 to +48
		18–35	−3±7	−14 to +9	−1±11	−16 to +22
ASUR	17	18–30	2±17	−12 to +33	−32±46	−82 to +25
		30–46	−3±1	−4 to −1	−62±10	−78 to −49
SPIRALE	1	15–26	−5±7	−17 to +5	0±19	−15 to +49
FIRS-2	1	13–20	+8±16	−12 to +31	+4±8	−6 to +17
		20–31	+5±7	−3 to +17	−18±156	−367 to 144

differences are observed in the comparison with FIRS-2, varying from −12 to +31 ppbv for 13–31 km, with typical values of +8 ppbv below 20 km and +5 ppbv above. Below 20 km, the relative differences are between −6% and +17%, but they increase significantly above 20 km. ACE-FTS is smaller than FIRS-2 between 11 and 13 km, and between 27 and 30 km.

The last set of comparisons is with N_2O partial columns measured by the ground-based FTIRs. Agreement is very good: the mean relative differences are within ±5.6% for eleven of the twelve stations. This mean relative difference is negative at ten stations, suggesting a small negative bias in the ACE-FTS partial columns over the altitude regions compared. Excellent correlation (R=0.964) is observed between the ACE-FTS and FTIR partial columns, with a slope of 1.01 and an intercept −0.20 on the line fitted to the data.

To assess the altitude range over which the ACE-FTS data quality is sufficient to detect the natural variability of N_2O, we can compare the ACE-FTS VMR statistical fitting errors (i.e., random errors) to the natural variability represented by the relative standard deviations on the mean profiles plotted in panel (d) of Figs. 1 to 7. As noted in Sect. 2, the fitting errors have a median value of <3% from 5–45 km, increasing to 17% at 60 km, with a mean of <4% from 5–35 km, oscillating above this due to some outliers in the individual percent fitting errors. Examining Figs. 1d and 3d, as these show results for the largest data sets (1099 and 6876 coincidences respectively), the ACE-FTS relative standard deviations are greater than the median fitting errors at all altitudes. This indicates that the data quality should be sufficient to detect the natural variability of N_2O over the entire altitude range examined, 5–60 km.

To assess the altitude range over which the ACE-FTS data quality is sufficient to measure the absolute VMR, we must rely on the differences relative to the other instruments, as there is no systematic error budget for the v2.2 data product. However, work is underway to produce an error budget for the next version to be released (v3.0). The mean absolute and relative differences given in Table 4 and Fig. 12, are therefore our best estimates of the absolute data quality.

Overall, the quality of the ACE-FTS version 2.2 N_2O VMR profiles is good over the entire altitude range of 5 to 60 km, although it is difficult to give an accurate assessment of the data quality at the lowest altitudes due to the small number of comparison datasets available. Between 6 and 30 km, the mean absolute differences for the satellite comparisons lie between −42 ppbv and +17 ppbv, with most within ±20 ppbv. This corresponds to relative deviations from the mean that are within ±15%, except for comparisons with MIPAS near 30 km, for which they are as large as 22.5%.

Between 18 and 30 km, the mean absolute differences are generally within ±10 ppbv, again excluding the aircraft and balloon comparisons. From 30 to 60 km, the mean absolute differences are within ±4 ppbv, and are mostly between −2 and +1 ppbv. Given the small N_2O VMR in this region, the relative deviations from the mean are therefore large at these altitudes, with most suggesting a negative bias in the ACE-FTS data between 30 and 50 km.

Acknowledgements. Funding for the ACE mission was provided primarily by the Canadian Space Agency (CSA) and the Natural Sciences and Engineering Research Council (NSERC) of Canada. This work was also supported by a grant from the CSA.

Odin is a Swedish-led satellite project funded jointly by the Swedish National Space Board (SNSB), the CSA, the Centre National d'Études Spatiales (CNES) in France and the National Technology Agency of Finland (Tekes).

Thanks to B. Bojkov of the Aura Validation Data Center (AVDC) and the Aura-MLS Data Distribution Team for access to the Aura-MLS dataset (see http://avdc.gsfc.nasa.gov). Work at the Jet Propulsion Laboratory, California Institute of Technology, is carried out under a contract with the National Aeronautics and Space Administration (NASA).

The IMK-IAA team thanks the European Space Agency (ESA) for providing MIPAS level 1 and 2 datasets. We would also like to acknowledge the following people for their work on the MIPAS data relevant to this validation study: T. von Clarmann, U. Grabowski, S. Kellmann, M. Kiefer, A. Linden, M. Milz, and T. Steck from IMK, and B. Funke and M. López-Puertas from IAA.

The ASUR group would like to acknowledge help and support from H. Bremer, A. Kleinböhl and G. Naeveke.

The SPIRALE balloon measurements could only be performed thanks to the technical team (L. Pomathiod, B. Gaubicher, G. Jannet); the flight was funded by ESA and the French space agency CNES for the Envisat validation project; the CNES balloon launching team is greatly acknowledged for successful operations. A. Hauchecorne is acknowledged for making available the use of MIMOSA advection model and F. Coquelet for useful help in the PV calculations and ACE data formatting.

The FIRS-2 work was funded by the NASA Upper Atmosphere Program, and the launch was supported both by the NASA Columbia Scientific Balloon Facility and the Swedish Space Corporation.

All of the ground-based FTIR stations operate within the framework of the Network for the Detection of Atmospheric Composition Change (NDACC, see http://www.ndacc.org), and are nationally funded and supported. The European ground-based FTIR stations have been supported partly by the EU projects UFTIR (http://www.nilu.no/uftir), GEOMON, and HYMN. National support by the Helmholtz Association within the project PEP is acknowledged for Ny-Ålesund and Bremen. The University of Bremen also acknowledges financial support from the ESA project TASTE. The Harestua measurements were also supported by the Swedish Environmental Agency. The support by the local IRF Kiruna staff is highly appreciated. The Belgian contributions to the present effort were partly supported by the ProDEx projects ACE, CINAMON and Envisat Database. Thanks are extended to the "International Foundation High Altitude Research Stations Jungfraujoch and Gornergrat" (HFSJG, Bern, Switzerland) for hosting the Liège FTIR laboratory and for providing accommodation for the observers at the Jungfraujoch site. The National Center for Atmospheric Research is supported by the National Science Foundation. The NCAR FTIR observation program at Thule, Greenland is supported under contract by NASA. Work at the Toronto Atmospheric Observatory was supported by NSERC, CSA, CFCAS, ABB Bomem, the Ontario Research and Development Challenge Fund, the Premier's Excellence Research Award and the University of Toronto.

Edited by: A. Richter

References

Abrams, M. C., Chang, A. Y., Gunson, M. R., Abbas, M. M., Goldman, A., Irion, F. W., Michelsen, H. A., Newchurch, M. J. Rinsland, C. P., Stiller, G. P., and Zander, R.: On the assessment and uncertainty of atmospheric trace gas burden measurements with high resolution infrared solar occultation spectra from space by the ATMOS experiment, Geophys. Res. Lett., 23, 17, 2337–2340, doi:10.1029/96GL01794, 1996.

Avallone, L. M. and Prather, M. J.: Photochemical evolution of ozone in the lower tropical stratosphere, J. Geophys. Res., 101, 1457–1461, 1996.

Avallone, L. M. and Prather, M. J.: Tracer-tracer correlations: Three dimensional model simulations and comparisons to observations, J. Geophys. Res., 102, 19 233–19 246, 1997.

Barbe, A. and Marche, P.: Obtention du profil de concentration de N_2O a partir de mesures dans le domaine infrarouge faites a partir sol, C. R. Acad. Sci. Paris, 300, 63–66, 1985.

Bates, D. R. and Hays, P. B.: Atmospheric nitrous oxide, Planet. Space Sci., 15, 189–198, 1967.

Battle, M., Bender, M., Sowers, T., Tans, P. P., Butler, J. H., Elkins, J. W., Conway, T., Zhang, N., Lang, P., and Clarke, A. D.: Atmospheric gas concentrations over the past century measured in air from firn at South Pole, Nature, 383, 231–235, 1996.

Bernath, P. F., McElroy, C. T., Abrams, M. C., Boone, C. D., Butler, M., Camy-Peyret, C., Carleer, M., Clerbaux, C., Coheur, P.-F., Colin, R., DeCola, P., De Mazière, M., Drummond, J. R., Dufour, D., Evans, W. F. J., Fast, H., Fussen, D., Gilbert, K., Jennings, D. E., Llewellyn, E. J., Lowe, R. P., Mahieu, E., McConnell, J. C., McHugh, M., McLeod, S. D., Michaud, R., Midwinter, C., Nassar, R., Nichitiu, F., Nowlan, C., Rinsland, C. P., Rochon, Y. J., Rowlands, N., Semeniuk, K., Simon, P., Skelton, R., Sloan, J. J., Soucy, M.-A., Strong, K., Tremblay, P., Turnbull, D., Walker, K. A., Walkty, I., Wardle, D. A., Wehrle, V., Zander, R., and Zou, J.: Atmospheric Chemistry Experiment (ACE): Mission overview, Geophys. Res. Lett., 32, L15S01, doi:10.1029/2005GL022386, 2005.

Bernath, P. F.: Atmospheric chemistry experiment (ACE): Analytical chemistry from orbit, TRAC-Trend. Anal. Chem., 5, 7, 647–654, 2006.

Blumenstock, T., Kopp, G., Hase, F., Hochschild, G., Mikuteit, S., Raffalski, U., and Ruhnke, R.: Observation of unusual chlorine activation by ground-based infrared and microwave spectroscopy in the late Arctic winter 2000/01, Atmos. Chem. Phys., 6, 897–905, 2006.

Boone, C. D., Nassar, R., Walker, K. A., Rochon, Y., McLeod, S. D., Rinsland, C. P., and Bernath, P. F.: Retrievals for the Atmospheric Chemistry Experiment Fourier-Transform Spectrometer, Appl. Optics, 44, 33, 7218–7231, 2005.

Boering, K. A., Daube, B. C., Wofsy, S. C., Loewenstein, M., Podolske, J. R., and Keim, E. R.: Tracer-tracer relationships and lower stratospheric dynamics: CO_2 and N_2O correlations during SPADE, Geophys. Res. Lett., 21, 2567–2570, 1994.

Brasseur, G. P. and Solomon, S.: Aeronomy of the Middle Atmosphere, 3rd ed., Springer, Dordrecht, The Netherlands, 644 pp., 2005.

Bregman, B., Lelieveld, J., van de Broek, M., Siegmund, P., Fischer, H., and Bujok, O.: N_2O and O_3 relationship in the lowermost stratosphere: A diagnostic for mixing processes as represented by a three-dimensional chemistry-transport model, J. Geophys. Res., 105, 17 279–17 290, 2000.

Bremer, H., von König, M., Kleinböhl, A., Küllmann, H., Künzi, K., Bramstedt, K., Burrows, J. P., Eichmann, K.-U., Weber, M., and Goede A. P. H.: Ozone depletion observed by the Airborne Sub-millimeter Radiometer (ASUR) during the Arctic winter 1999/2000, J. Geophys. Res., 107, D20, 8277, doi:10.1029/2001JD000546, 2002.

Buchwitz, M., Schneising, O., Burrows, J. P., Bovensmann, H., Reuter, M., and Notholt, J.: First direct observation of the atmospheric CO_2 year-to-year increase from space, Atmos. Chem. Phys., 7, 4249–4256, 2007.

Canty, T., Pickett, H. M., Salawitch, R. J., Jucks, K. W., Traub, W. A., and Waters, J. W.: Stratospheric and mesospheric HO_x: results from Aura-MLS and FIRS-2, Geophys. Res. Lett., 33, L12802, doi:10.1029/2006GL025964, 2006.

Crutzen, P. J.: The influence of nitrogen oxides on the atmospheric ozone content, Q. J. Roy. Meteor. Soc., 96, 320–325, 1970.

Dils, B., De Mazière, M., Müller, J. F., Blumenstock, T., Buchwitz, M., de Beek, R., Demoulin, P., Duchatelet, P., Fast, H., Frankenberg, C., Gloudemans, A., Griffith, D., Jones, N., Kerzenmacher, T., Kramer, I., Mahieu, E., Mellqvist, J., Mittermeier, R. L., Notholt, J., Rinsland, C. P., Schrijver, H., Smale, D., Strandberg, A., Straume, A. G., Stremme, W., Strong, K., Sussmann, R., Taylor, J., van den Broek, M., Velazco, V., Wagner, T., Warneke, T., Wiacek, A., and Wood, S.: Comparisons between SCIAMACHY and ground-based FTIR data for total columns of CO, CH_4, CO_2 and N_2O, Atmos. Chem. Phys., 6, 1953–1976, 2006.

Drummond, J. R., Houghton, J. T., Peskett, G. D., Rodgers, C. D., Wale, M. J., Whitney, J., and Williamson, E. J.: The stratospheric and mesospheric sounder on NIMBUS-7, Philos. T. Roy. Soc. A, A296, 219–241, 1980.

Dupuy, E., Walker, K. A., Kar, J., Boone, C. D., McElroy, C. T., Bernath, P. F., Drummond, J. R., Skelton, R., McLeod, S. D., Hughes, R. C., Nowlan, C. R., Dufour, D. G., Zou, J., Nichitiu, F., Strong, K., Baron, P., Bevilacqua, R. M., Blumenstock, T., Bodeker, G. E., Borsdorff, T., Bourassa, A. E., Bovensmann, H., Boyd, I. S., Bracher, A., Brogniez, C., Burrows, J. P., Catoire, V., Ceccherini, S., Chabrillat, S., Christensen, T., Coffey, M. T., Cortesi, U., Davies, J., Clercq, C. D., Degenstein, D. A., De Mazière, M., Demoulin, P., Dodion, J., Firanski, B., Fischer, H., Forbes, G., Froidevaux, L., Fussen, D., Gerard, P., Godin-Beekman, S., Goutail, F., Granville, J., Griffith, D., Haley, C. S., Hannigan, J. W., Höpfner, M., Jin, J. J., Jones, A., Jones, N. B., Jucks, K., Kagawa, A., Kasai, Y., Kerzenmacher, T. E., Kleinböhl, A., Klekociuk, A. R., Kramer, I., Küllmann, H., Kuttippurath, J., Kyrölä, E., Lambert, J. C., Livesey, N. J., Llewellyn, E. J., Lloyd, N. D., Mahieu, E., Manney, G. L., Marshall, B. T., McConnell, J. C., McCormick, M. P., McDermid, I. S., McHugh, M., McLinden, C. A., Mellqvist, J., Mizutani, K., Murayama, Y., Murtagh, D. P., Oelhaf, H., Parrish, A., Petelina, S. V., Piccolo, C., Pommereau, J. P., Randall, C. E., Robert, C., Roth, C., Russell III, J. M., Schneider, M., Senten, C., Steck, T., Strandberg, A., Strawbridge, K. B., Sussmann, R., Swart, D. P. J., Tarasick, D. W., Taylor, J. R., Tétard, C., Thomason, L. W., Thompson, A. M., Tully, M. B., Urban, J., Vanhellemont, F., von Clarmann, T., von der Gathen, P., von Savigny, C., Waters, J. W., Witte, J. C., Wolff, M., and Zawodny, J. M.: Validation of ozone measurements from the Atmospheric Chemistry Experiment (ACE), Atmos. Chem. Phys. Discuss., 8, 2513–2656, 2008, http://www.atmos-chem-phys-discuss.net/8/2513/2008/.

Ejiri, M. K., Terao, Y., Sugita, T., Nakajima, H., Yokota, T., Toon, G. C., Sen, B., Wetzel, G., Oelhaf, H., Urban, J., Murtagh, D., Irie, H., Saitoh, N., Tanaka, T., Kanzawa, H., Shiotani, M., Aoki, S., Hashida, G., Machida, T., Nakazawa, T., Kobayashi, H., and Sasano, Y.: Validation of the Improved Limb Atmospheric Spectrometer-II (ILAS-II) Version 1.4 nitrous oxide and methane profiles, J. Geophys. Res., 111, D22S90, doi:10.1029/2005JD006449, 2006.

Fischer, H., Birk, M., Blom, C., Carli, B, Carlotti, M., von Clarmann, T., Delbouille, L., Dudhia, A., Ehhalt, D., Endemann, M., Flaud, J. M., Gessner, R., Kleinert, A., Koopmann, R., Langen, J., López-Puertas, M., Mosner, P., Nett, H., Oelhaf, H., Perron, G., Remedios, J., Ridolfi, M., Stiller, G., and Zander, R.: MIPAS: an instrument for atmospheric and climate research, Atmos. Chem. Phys., 8, 2151–2188, 2008.

Flückiger, J., Dällenbach, A., Blunier, T., Stauffer, B., Stocker, T. F., Raynaud, D., and Barnola, J.-M.: Variations in atmospheric N_2O concentration during abrupt climatic changes, Science, 285, 227–230, 1999.

Froidevaux, L., Livesey, N. J., Read, W. G., Jiang, Y. B., Jimenez, C., Filipiak, M. J., Schwartz, M. J., Santee, M. L., Pumphrey, H. C., Jiang, J. H., Wu, D. L., Manney, G. L., Drouin, B. J., Waters, J. W., Fetzer, E. J., Bernath, P. F., Boone, C. D., Walker, K. A., Jucks, K. W., Toon, G. C., Margitan, J. J., Sen, B., Webster, C. R., Christensen, L. E., Elkins, J. W., Atlas, E., Lueb, R. A., and Hendershot, R.: Early Validation Analyses of Atmospheric Profiles From EOS MLS on the Aura Satellite, IEEE T. Geosci. Remote, 44, 5, 1106–1121, 2006.

Glatthor, N., von Clarmann, T., Fischer, H., Funke, B., Grabowski, U., Höpfner, M., Kellmann, S., Kiefer, M., Linden, A., Milz, M., Steck, T., Stiller, G. P., Mengistu Tsidu, G., and Wang, D. Y.: Mixing processes during the Antarctic vortex split in September/October 2002 as inferred from source gas and ozone distributions from ENVISAT-MIPAS, J. Atmos. Sci., 62, 787–800, 2005.

Goldman, A., Paton-Walsh, C., Bell, W., Toon, G. C., Blavier, J. F., Sen, B., Coffey, M. T., Hannigan, J. W., and Mankin, W. G.: Network for the Detection of Stratospheric Change Fourier transform infrared intercomparison at Table Mountain Facility, November 1996, J. Geophys. Res., 104, D23, 30 481–30 503, 1999.

Griesfeller, A., Griesfeller, J., Hase, F., Kramer, I., Loes, P., Mikuteit, S., Raffalski, U., Blumenstock, T., and Nakajima, H.: Comparison of ILAS-II and ground-based FTIR measurements

of O_3, HNO_3, N_2O, and CH_4 over Kiruna, Sweden, J. Geophys. Res., 111, D11, doi:10.1029/2005JD006451, 2006.

Griffith, D. W. T., Jones, N. B., McNamara, B., Paton-Walsh, C., Bell, W., and Bernardo, C.: Intercomparison of ground-based solar FTIR measurements of atmospheric trace gases at Lauder, New Zealand, J. Ocean. Atmos. Tech., 20, 8, 1138–1153, 2003.

Gunson, M. R., Abbas, M. M., Abrams, M. C., Allen, M., Brown, L. R., Brown, T. L., Chang, A. Y., Goldman, A., Irion, F. W., Lowes, L. L., Mahieu, E., Manney, G. L., Michelsen, H. A., Newchurch, M. J., Rinsland, C. P., Salawitch, R. J., Stiller, G. P., Toon, G. C., Yung, Y. L., and Zander, R.: The Atmospheric Trace Molecule Spectroscopy (ATMOS) experiment: Deployment on the ATLAS Space Shuttle missions, Geophys. Res. Lett., 23, 2333–2336, 1996.

Hase, F.: Inversion von Spurengasprofilen aus hochaufgelösten bodengebundenen FTIR-Messungen in Absorption, Wissenschaftliche Berichte Forschungszentrum Karlsruhe, FZKA 6512, ISSN 0947-8620, 2000.

Hase, F., Hannigan, J. W., Coffey, M. T., Goldman, A., Höpfner, M., Jones, N. B., Rinsland, C. P., and Wood, S. W.: Intercomparison of retrieval codes used for the analysis of high-resolution, ground-based FTIR measurements, J. Quant. Spectrosc. Ra., 87, 25–52, 2004.

Hauchecorne, A., Godin, S., Marchand, M., Heese, B., and Souprayen, C.: Quantification of the transport of chemical constituents from the polar vortex to midlatitudes in the lower stratosphere using the high-resolution advection model MIMOSA and effective diffusivity, J. Geophys. Res., 107, D20, 8289, doi:10.1029/2001JD000491, 2002.

Hegglin, M. I., Brunner, D., Peter, T., Hoor, P., Fischer, H., Staehelin, J., Krebsbach, M., Schiller, C., Parchatka, U., and Weers, U.: Measurements of NO, NO_y, N_2O, and O_3 during SPURT: implications for transport and chemistry in the lowermost stratosphere, Atmos. Chem. Phys., 6, 1331–1350, 2006.

Hirsch, A. I., Michalak, A. M., Bruhwiler, L. M., Peters, W., Dlugokencky, E. J., and Tans P. P.: Inverse modeling estimates of the global nitrous oxide surface flux from 1998–2001, Global Biogeochem. Cy., 20, GB1008, doi:10.1029/2004GB002443, 2006.

Holland, E. A., Braswell, B. H., Sulzman, J., and Lamarque, J. F.: Nitrogen deposition onto the United States and Western Europe: synthesis of observations and models, Ecol. Appl., 15, 38–57, 2005.

Holton, J. R.: A dynamically based transport parameterization for one-dimensional photochemical models of the stratosphere, J. Geophys. Res., 91, 2681–2686, 1986.

Intergovernmental Panel on Climate Change (IPCC): Climate Change 2007: The Physical Science Basis. Contribution of Working Group I to the Fourth Assessment Report of the Intergovernmental Panel on Climate Change, edited by: Solomon, S., Qin, D., Manning, M., Chen, Z., Marquis, M., Averyt, K. B., Tignor M., and Miller, H. L., Cambridge University Press, Cambridge, UK and New York, NY, USA, 996 pp., 2007.

Irion, F. W., Gunson, M. R., Toon, G. C., Chang, A. Y., Eldering, A., Mahieu, E., Manney, G. L., Michelsen, H. A., Moyer, E. J., Newchurch, M. J., Osterman, G. B., Rinsland, C. P., Salawitch, R. J., Sen, B., Yung, Y. L., and Zander, R.: Atmospheric Trace Molecule Spectroscopy (ATMOS) Experiment Version 3 data retrievals, Appl. Optics, 41, 33, 6968–6979, 2002.

Johnson, D. G., Jucks, K. W., Traub, W. A., and Chance, K. V.: Smithsonian stratospheric far-infrared spectrometer and data reduction system, J. Geophys. Res., 100, D2, 3091–3106, 1995.

Jones, R. L. and Pyle, J. A.: Observations of CH_4 and N_2O by the Nimbus 7 SAMS: A comparison with in situ data and two-dimensional numerical model calculations, J. Geophys. Res., 89, 5263–5279, 1984.

Jones, R. L., Pyle, J. A., Harries, J. E., Zavody, A. M., Russell III, J. M. and Gille, J. C.: The water vapor budget of the stratosphere studied using LIMS and SAMS satellite data, Q. J. Roy. Meteor. Soc., 112, 1127–1143, 1986.

Jucks, K. W., Johnson, D. G., Chance, K. V., Traub, W. A., Margitan, J. M., Stachnik, R., Sasano, Y., Yokota, T., Kanzawa, H., Shibasaki, K., Suzuki, M., and Ogawa, T.: Validation of ILAS v5.2 data with FIRS-2 balloon observations, J. Geophys. Res., 107, D24, 8207, doi:10.1029/2001JD000578, 2002.

Kanzawa, H., Sugita, T., Nakajima, H., Bodeker, G. E., Oelhaf, H., Stowasser, M., Wetzel, G., Engel, A., Schmidt, U., Levin, I., Toon, G. C., Sen, B., Blavier, J.-F., Aoki, S., Nakazawa, T., Jucks, K. W., Johnson, D. G., Traub, W. A., Camy-Peyret, C., Payan, S., Jeseck, P., Murata, I., Fukunishi, H., von König, M., Bremer, H., Küllmann, H., Park, J. H., Pan, L. L., Yokota, T., Suzuki, M., Shiotani, M., and Sasano Y.: Validation and data characteristics of nitrous oxide and methane profiles observed by the Improved Limb Atmospheric Spectrometer (ILAS) and processed with the Version 5.20 algorithm, J. Geophys. Res., 108, 8003, doi:10.1029/2002JD002458, 2003.

Khosrawi, F., Müller, R., Proffitt, M. H., and Nakajima, H.: Monthly averaged ozone and nitrous oxide from the Improved Limb Atmospheric Spectrometer (ILAS) in the Northern and Southern Hemisphere polar regions, J. Geophys. Res., 109, D10301, doi:10.1029/2003JD004365, 2004.

Khosrawi, F., Müller, R., Proffitt, M. H., and Nakajima, H.: Monthly averages of nitrous oxide and ozone for the Northern and Southern Hemisphere high latitudes: A "1-year climatology" derived from ILAS/ILAS-II observations, J. Geophys. Res., 111, D11S11, doi:10.1029/2005JD006384, 2006.

Kuttippurath, J.: Study of stratospheric composition using airborne submillimter radiometry and a chemical transport model, Ph.D. Thesis, ISBN 3-8325-1069-9, ISSN 1615-6862, Logos Verlag, Berlin, 2005.

Kurylo, M. J. and Zander, R. J.: The NDSC – Its status after ten years of operation, in: Proceedings of the Quadrennial Ozone Symposium, edited by: Bojkov, R. D. and Kazuo, S., Sapporo, Japan, 3–8 July 2000, 137–138, 2000.

Lambert, A., Read, W. G., Livesey, N. J., Santee, M. L., Manney, G. L., Froidevaux, L., Wu, D. L., Schwartz, M. J., Pumphrey, H. C., Jimenez, C., Nedoluha, G. E., Cofield, R. E., Cuddy, D. T., Daffer, W. H., Drouin, B. J., Fuller, R. A., Jarnot, R. F., Knosp, B. W., Pickett, H. M., Perun, V. S., Snyder, W. V., Stek, P. C., Thurstans, R. P., Wagner, P. A., Waters, J. W., Jucks, K. W., Toon, G. C., Stachnik, R. A., Bernath, P. F., Boone, C. D., Walker, K. A., Urban, J., Murtagh, D., Elkins, J. W., and Atlas, E.: Validation of the Aura Microwave Limb Sounder middle atmosphere water vapor and nitrous oxide measurements, J. Geophys. Res., 112, D24S36, doi:10.1029/2007JD008724, 2007.

Livesey, N. J., Van Snyder, W., Read, W. J., and Wagner, P. A.: Retrieval algorithms for the EOS Microwave Limb Sounder (MLS), IEEE T. Geosci. Remote, 44, 5, 1144–1155, doi:10.1109/TGRS.2006.872327, 2006.

Livesey, N. J., Read, W. G., Lambert, A., Cofield, R. E., Cuddy, D. T., Froidevaux, L., Fuller, R. A., Jarnot, R. F., Jiang, J. H., Jiang, Y. B., Knosp, B. W., Kovalenko, L. J., Pickett, H. M., Pumphrey, H. C., Santee, M. L., Schwartz, M. J., Stek, P. C., Wagner, P. A., Waters, J. W., and Wu, D. L.: Earth Observing System (EOS) – Aura Microwave Limb Sounder (MLS), Version 2.2 Level 2 data quality and description document, Tech. Rep. JPL D-33509, Jet Propulsion Laboratory, California Institute of Technology, 2007.

Mahlman, J. D., Levy III, H., and Moxim, W. J.: Three-dimensional simulations of stratospheric N_2O: Predictions for other trace constituents, J. Geophys. Res., 91, 2687–707, 1986.

Mahieu, E., Zander, R., Delbouille, L., Demoulin, P., Roland, G., and Servais, C.: Observed trends in total vertical column abundances of atmospheric gases from IR solar spectra recorded at the Jungfraujoch, J. Atmos. Chem., 28, 227–243, 1997.

McElroy, M. B. and McConnell, J. C.: Nitrous oxide: Natural source of stratospheric NO, J. Atmos. Sci., 28, 1095–1103, 1971.

McElroy, C. T., Nowlan, C. R., Drummond, J. R., Bernath, P. F., Barton, D. V., Dufour, D. G., Midwinter, C., Hall, R. B., Ogyu, A., Ullberg, A., Wardle, D. I., Kar, J., Zou, J., Nichitiu, F., Boone, C. D., Walker, K. A., and Rowlands, N.: The ACE-MAESTRO instrument on SCISAT: Description, performance, and preliminary results, Appl. Optics, 46, 20, 4341–4356, 2007.

McLinden, C. A., Prather, M. J., and Johnson, M. S.: Global modeling of the isotopic analogues of N_2O: Stratospheric distributions, budgets, and the ^{17}O–^{18}O mass-independent anomaly, J. Geophys. Res., 108, D8, 4233, doi:10.1029/2002JD002560, 2003.

Michelsen, H. A., Manney, G. L., Gunson, M. R., and Zander, R.: Correlations of stratospheric abundances of NO_y, O_3 , N_2O, and CH_4 derived from ATMOS measurements, J. Geophys. Res., 103, 28 347–28 359, 1998.

Minschwaner, K., Dessler, A. E., Elkins, J. W., Volk, C. M., Fahey, D. W., Loewenstein, M., Podolske, J. R., Roche, A. E. and Chan, K. R.: Bulk properties of isentropic mixing into the tropics in the lower stratosphere, J. Geophys. Res., 101, 9433–9439, 1996.

Moreau, G., Robert, C., Catoire, V., Chartier, M., Camy-Peyret, C., Huret, N., Pirre, M., Pomathiod, L., and Chalumeau, G.: SPIRALE: a multispecies in situ balloon-borne instrument with six tunable diode laser spectrometers, Appl. Optics, 44, 28, 5972–5989, 2005.

Müller, R., Crutzen, P. J., Groo, J.-U., Brühl, C., Russell III, J. M., and Tuck, A. F.: Chlorine activation and ozone depletion in the Arctic vortex: Observations by the Halogen Occultation Experiment on the Upper Atmosphere Research Satellite, J. Geophys. Res., 101, 12 531–12 554, 1996.

Murphy, D. M., Fahey, D. W., Proffitt, M. H., Liu, C. S., Chan, K. R., Eubank, C. S., Kawa, S. R., and Kelly, K. K.: Reactive nitrogen and its correlation with ozone in the lower stratosphere and upper troposphere, J. Geophys. Res., 98, 8751–8773, 1993.

Murtagh, D. P., Frisk, U., Merino, F., Ridal, M., Jonsson, A., Stegman, J., Witt, G., Eriksson, P., Jiménez, C., Mégie, G., de La Noë, J., Ricaud, P., Baron, P., Pardo, J. R., Hauchcorne, A., Llewellyn, E. J., Degenstein, D. A., Gattinger, R. L., Lloyd, N. D., Evans, W. F. J., McDade, I. C., Haley, C. S., Sioris, C., von Savigny, C., Solheim, B. H., McConnell, J. C., Strong, K., Richardson, E. H., Leppelmeier, G. W., Kyrölä, E., Auvinen, H., and Oikarinen, L.: An overview of the Odin atmospheric mission, Can. J. Phys., 80, 309–319, 2002.

Nakajima, H., Suzuki, M., Matsuzaki, A., Ishigaki, T., Waragai, K., Mogi, Y., Kimura, N., Araki, N., Yokota, T., Kanzawa, H., Sugita, T., and Sasano, Y.: Characteristics and performance of the Improved Limb Atmospheric Spectrometer (ILAS) in orbit, J. Geophys. Res., 107, D24, 8213, doi:10.1029/2001JD001439, 2002.

Nash E. R., Newman, P. A., Rosenfield, J. E., and Schoeberl, M. R.: An objective determination of the polar vortex using Ertel's potential vorticity, J. Geophys. Res., 101, 9471–9478, 1996.

Notholt, J., Toon, G. C., Stordal, F., Solberg S., Schmidbauer, N., Becker, E., Meier, A., and Sen, B.: Seasonal variations of atmospheric trace gases in the high Arctic at 79° N, J. Geophys. Res., 102, 12 855–12 861, 1997.

Offermann, D., Grossmann, K.-U., Barthol, P., Knieling, P., Riese, M., and Trant, R.: Cryogenic Infrared Spectrometers and Telescopes for the Atmosphere (CRISTA) experiment and middle atmosphere variability, J. Geophys. Res., 104, 16 311–16 3251, 1999.

Paton-Walsh, C., Bell, W., Gardiner, T., Swann, N., Woods, P., Notholt, J., Schutt, H., Galle, B., Arlander, W., and Mellqvist, J.: An uncertainty budget for ground-based Fourier transform infrared column measurements of HCl, HF, N_2O, and HNO_3, deduced from results of side-by-side instrument intercomparisons, J. Geophys. Res., 102, 867–887, 1997.

Paton-Walsh, C., Jones, N. B., Wilson, S. R., Haverd, V., Meier, A., Griffith, D. W. T., and Rinsland, C. P.: Measurements of trace gas emissions from Australian forest fires and correlations with coincident measurements of aerosol optical depth, J. Geophys. Res., 110, D24305, doi:24310.21029/22005JD006202, 2005.

Piccolo, C. and Dudhia, A.: Precision validation of MIPAS-Envisat products, Atmos. Chem. Phys., 7, 1915–1923, 2007.

Plumb, R. A. and Ko, M. K. W.: Interrelationships between mixing ratios of long-lived stratospheric constituents, J. Geophys. Res., 97, 10 145–10 156, 1992.

Plumb, R. A.: A "tropical pipe" model of stratospheric transport, J. Geophys. Res., 101, 3957–3972, 1996.

Pougatchev, N. S. and Rinsland, C. P.: Spectroscopic study of the seasonal variation of carbon monoxide vertical distribution above Kitt Peak, J. Geophys. Res., 100, 1409–1416, 1995.

Pougatchev, N. S., Connor, B. J., and Rinsland, C. P.: Infrared measurements of the ozone vertical distribution above Kitt Peak, J. Geophys. Res., 100, 16 689–16 697, 1995.

Proffitt, M. H., Fahey, D. W., Kelly, K. K., and Tuck, A. F.: High-latitude ozone loss outside the Antarctic ozone hole, Nature, 342, 233–237, 1989.

Proffitt, M. H., Margitan, J. J., Kelly, K. K., Loewenstein, M., Podolske, J. R., and Chan, K. R.: Ozone loss in the Arctic polar vortex inferred from high-altitude aircraft measurements, Nature, 347, 31–36, 1990.

Proffitt, M., Loewenstein, M., and Solomon, S.: Comparison of 2-D model simulations of ozone and nitrous oxide at high latitudes with stratospheric measurements, J. Geophys. Res., 97, 939–944, 1992.

Ramanathan, V., Cicerone, R. J., Singh, H. B., and Kiehl, J. T.: Trace gas trends and their potential role in climate change, J. Geophys. Res., 90, 5547–5566, 1985.

Randel, W., Gille, J., Roche, A., Kumer, J., Mergenthaler, J., Waters, J., Fishbein, E., and Lahoz, W.: Stratospheric transport from the tropics to middle latitudes by planetary-wave mixing, Nature,

365, 533–535, 1993.

Randel, W., Boville, B., Gille, J., Bailey, P., Massie, S., Kumer, J., Mergenthaler, J., and Roche, A.: Simulation of stratospheric N_2O in the NCAR CCM2: Comparison with CLAES data and global budget analyses, J. Atmos. Sci., 51, 2834–2845, 1994.

Raspollini, P., Belotti, C., Burgess, A., Carli, B., Carlotti, M., Ceccherini, S., Dinelli, B. M., Dudhia, A., Flaud, J.-M., Funke, B., Höpfner, M., López-Puertas, M., Payne, V., Piccolo, C., Remedios, J. J., Ridolfi, M., and Spang, R.: MIPAS level 2 operational analysis, Atmos. Chem. Phys., 6, 5605–5630, 2006.

Remedios, J. J., Ruth, S. L., Rodgers, C. D., Taylor, R. W., Roche, A. E., Gille, J. C., Gunson, M. R., Russell III, J. M., Park, J., Zipf, E. C., and Erdman, P. W.: Measurements of CH_4 and N_2O distributions by the ISAMS: Retrieval and validation, J. Geophys. Res., 101, 9843–9871, 1996.

Ridolfi, M., Carli, B., Carlotti, M., von Clarmann, T., Dinelli, B. M., Dudhia, A., Flaud, J.-M., Hpfner, M., Morris, P. E., Raspollini, P., Stiller, G., and Wells, R. J.: Optimized forward model and retrieval scheme for MIPAS near-real-time data processing, Appl. Optics, 39, 1323–1340, 2000.

Riese, M., Spang, R., Preusse, P., Ern, M., Jarisch, M., Offermann, D., and Grossmann, K. U.: Cryogenic Infrared Spectrometers and Telescopes for the Atmosphere (CRISTA) data processing and atmospheric temperature and trace gas retrieval, J. Geophys. Res., 104, D13, 16 349–16 368, 1999.

Rinsland, C. P., Jones, N. B., Connor, B. J., Logan, J. A., Pougatchev, N. S., Goldman, A., Murcray, F. J., Stephen, T. M., Pine, A. S., Zander, R., Mahieu, E., and Demoulin, P.: Northern and southern hemisphere ground-based infrared spectroscopic measurements of tropospheric carbon monoxide and ethane, J. Geophys. Res., 103, 28 197–28 217, 1998.

Roche, A., Kumer, J., Mergenthaler, J., Ely, G., Uplinger, W., Potter, J., James, T., and Sterritt, L.: The Cryogenic Limb Array Etalon Spectrometer (CLAES) on UARS: Experiment description and performance, J. Geophys. Res., 98, 10 763–10 775, 1993.

Roche, A. E., Kumer, J. B., Nightingale, R. W., Mergenthaler, J. L., Ely, G. A., Bailey, P. L., Massie, S. T., Gille, J. C., Edwards, D. P., Gunson, M. R., Abrams, M. C., Toon, G. C., Webster, C. R., Traub, W. A., Jucks, K. W., Johnson, D. G., Murcray, D. G., Murcray, F. H., Goldman, A., and Zipf, E. C.: Validation of CH_4 and N_2O measurements by the cryogenic limb array etalon spectrometer instrument on the Upper Atmosphere Research Satellite, J. Geophys. Res., 101, D6, 9679–9710, 1996.

Rodgers, C. D.: Inverse Methods for Atmospheric Sounding: Theory and Practice, Volume 2 of Series on Atmospheric, Oceanic and Planetary Physics, World Scientific Co. Pte. Ltd., ISBN 981-02-2740-X, 2000.

Rodgers, C. D. and Connor, B. J.: Intercomparison of remote sounding instruments, J. Geophys. Res., 108, D3, 4116, doi:10.1029/2002JD002299, 2003.

Rothman, L. S., Barbe, A., Benner, D. C., Brown, L. R., Camy-Peyret, C., Carleer, M. R., Chance, K., Clerbaux, C., Dana, V., Devi, V. M., Fayt, A., Flaud, J.-M., Gamache, R. R., Goldman, A., Jacquemart, D., Jucks, K. W., Lafferty, W. J., Mandin, J.-Y., Massie, S. T., Nemtchinov, V., Newnham, D. A., Perrin, A., Rinsland, C. P., Schroeder, J., Smith, K. M., Smith, M. A. H., Tang, K., Toth, R. A., Vander Auwera, J., Varanasi, P., and Yoshino, K.: The HITRAN molecular spectroscopic database: edition of 2000 including updates through 2001, J. Quant. Spectrosc. Ra., 82, 5–44, 2003.

Rothman, L. S., Jacquemart, D., Barbe, A., Chris Benner, D., Birk, M., Brown, L. R., Carleer, M. R., Chackerian Jr., C., Chance, K., Coudert, L. H., Dana, V., Devi, V. M., Flaud, J.-M., Gamache, R. R., Goldman, A., Hartmann, J.-M., Jucks, K. W., Maki, A. G., Mandin, J.-Y., Massie, S. T., Orphal, J., Perrin, A., Rinsland, C. P., Smith, M. A. H., Tennyson, J., Tolchenov, R. N., Toth, R. A., Vander Auwera, J., Varanasi, P., and Wagner, G.: The HITRAN 2004 molecular spectroscopic database, J. Quant. Spectrosc. Ra., 96, 139–204, 2005.

Ruth, S. L., Remedios, J. J., Lawrence, B. N., and Taylor, F. W.: Measurements of N_2O by the UARS Improved Stratospheric and Mesospheric Sounder during the Early Northern Winter 1991/92, J. Atmos. Sci., 51, 20, 2818–2833, 1994.

Sankey, D. and Shepherd, T. G.: Correlations of long-lived chemical species in a middle atmosphere general circulation model, J. Geophys. Res., 108, D16, 4494, doi:10.1029/2002JD002799, 2003.

Schneider, M., Blumenstock, T., Chipperfield, M., Hase, F., Kouker, W., Reddmann, T., Ruhnke, R., Cuevas, E., and Fischer, H.: Subtropical trace gas profiles determined by ground-based FTIR spectroscopy at Izaña (28°,N, 16° W): Five year record, error analysis, and comparison with 3-D CTMs, Atmos. Chem. Phys., 5, 153–167, 2005.

Senten, C., De Mazire, M., Dils, B., Hermans, C., Kruglanski, M., Neefs, E., Scolas, F., Vandaele, A. C., Vanhaelewyn, G., Vigouroux, C., Carleer, M., Coheur, P. F., Fally, S., Barret, B., Baray, J. L., Delmas, R., Leveau, J., Metzger, J. M., Mahieu, E., Boone, C., Walker, K. A., Bernath, P. F., and Strong, K.: Technical Note: New ground-based FTIR measurements at Ile de La Réunion: observations, error analysis, and comparisons with independent data, Atmos. Chem. Phys., 8, 3483–3508, 2008, http://www.atmos-chem-phys.net/8/3483/2008/.

Sung, K., Skelton, R., Walker, K. A., Boone, C. D., Fu, D., and Bernath, P. F.: N_2O and O_3 arctic column amounts from PARIS-IR observations: Retrievals, characterization and error analysis, J. Quant. Spectrosc. Ra., 107, 385–406, 2007.

Sussmann, R. and Schäfer, K.: Infrared spectroscopy of tropospheric trace gases: combined analysis of horizontal and vertical column abundances, Appl. Optics., 36, 735–741, 1997.

Taylor, F. W., Rodgers, C. D., Whitney, J. G., Barnett, J. J., Peskett, G. D., Venters, P., Ballard, J., Palmer, C. W. P., Knight, R. J., Morris, P., Nightingale, T., and Dudhia, A.: Remote sensing of atmospheric structure and composition by pressure modulator radiometry from space: The ISAMS experiment on UARS, J. Geophys. Res., 98, D6, 10 799–10 814, 1993.

Toohey, M. and Strong, K.: Estimating biases and error variances through the comparison of coincident satellite measurements, J. Geophys. Res., 112, D13306, doi:10.1029/2006JD008192, 2007.

Urban, J., Lautié, N., Le Flochmoën, E., Murtagh, D., Ricaud, P., de La Noë, J., Dupuy, E., Drouin, A., El Amraoui, L., Eriksson, P., Frisk, U., Jiménez, C., Kyrölä, E., Llewellyn, E. J., Mégie, G., Nordh, L., and Olberg, M.: The Northern Hemisphere stratospheric vortex during the 2002–03 winter: Subsidence, chlorine activation and ozone loss observed by the Odin Sub-Millimetre Radiometer, Geophys. Res. Lett., 31, L07103, doi:10.1029/2003GL019089, 2004.

Urban, J., Lautié, N., Le Flochmoën, E., Jiménez, C., Eriksson,

P., de La Noë, J., Dupuy, E., El Amraoui, L., Frisk, U., Jégou, F., Murtagh, D., Olberg, M., Ricaud, P., Camy-Peyret, C., Dufour, G., Payan, S., Huret, N., Pirre, M., Robinson, A. D., Harris, N. R. P., Bremer, H., Kleinböhl, A., Küllmann, K., Künzi, K., Kuttippurath, J., Ejiri, M. K., Nakajima, H., Sasano, Y., Sugita, T., Yokota, T., Piccolo, C., Raspollini, P., and Ridolfi, M.: Odin/SMR limb observations of stratospheric trace gases: Validation of N_2O, J. Geophys. Res., 110, D09301, doi:10.1029/2004JD005394, 2005a.

Urban, J., Lautié, N., Le Flochmoën, E., Jiménez, C., Eriksson, P., Dupuy, E., El Amraoui, L., Ekström, M., Frisk, U., Murtagh, D., de La Noë, J., Olberg M., and Ricaud, P.: Odin/SMR Limb Observations of Stratospheric Trace Gases: Level 2 Processing of ClO, N_2O, O_3, and HNO_3, J. Geophys. Res., 110, D14307, doi:10.1029/2004JD005741, 2005b.

Urban, J., Murtagh, D., Lautié, N., Barret, B., Dupuy, E., de La Noë, J., Eriksson, P., Frisk, U., Jones, A., Le Flochmoën, E., Olberg, M., Piccolo, C., Ricaud, P., and Rösevall, J.: Odin/SMR Limb Observations of Trace Gases in the Polar Lower Stratosphere during 2004–2005, Proc. ESA First Atmospheric Science Conference, edited by: Lacoste, H., 8–12 May 2006, Frascati, Italy, ESA-SP-628, ISBN-92-9092-939-1, ISSN-1609-042X, 2006.

Vigouroux, C., De Mazière, M., Errera, Q., Chabrillat, S., Mahieu, E., Duchatelet, P., Wood, S., Smale, D., Mikuteit, S., Blumenstock, T., Hase, F., and Jones, N.: Comparisons between ground-based FTIR and MIPAS N_2O and HNO_3 profiles before and after assimilation in BASCOE, Atmos. Chem. Phys., 7, 377–396, 2007.

Volk, C. M., Elkins, J. W., Fahey, D. W., Salawitch, R. J., Dutton, G. S., Gilligan, J. M., Proffitt, M. H., Loewenstein, M., Podolske, J. R., Minschwaner, K., Margitan, J. J., and Chan, K. R.: Quantifying transport between the tropical and mid-latitude lower stratosphere, Science, 272, 1763–1768, 1996.

von Clarmann, T.: Validation of remotely sensed profiles of atmospheric state variables: strategies and terminology, Atmos. Chem. Phys., 6, 4311–4320, 2006.

von Koenig, M., Bremer, H., Eyring, V., Goede, A., Hetzheim, H., Kleipool, Q., Kuellmann, H., and Kuenzi, K.: An airborne submm radiometer for the observation of stratospheric trace gases: Microwave Radiometry and Remote Sensing of the Earth's Surface and Atmosphere, edited by: Pampaloni, P. and Paloscia, S., VSP Utrecht, 409–415, 2000.

Waters, J. W., Froidevaux, L., Harwood, R. S., Jarnot, R. F., Pickett, H. M., Read, W. G., Siegel, P. H., Cofield, R. E., Filipiak, M. J., Flower, D. A., Holden, J. R., Lau, G. K., Livesey, N. J., Manney, G. L., Pumphrey, H. C., Santee, M. L., Wu, D. L., Cuddy, D. T., Lay, R. R., Loo, M. S., Perun, V. S., Schwartz, M. J., Stek, P. C., Thurstans, R. P., Boyles, M. A., Chandra, K. M., Chavez, M. C., Chen, G.-S., Chudasama, B. V., Dodge, R., Fuller, R. A., Girard, M. A., Jiang, J. H., Jiang, Y., Knosp, B. W., LaBelle, R. C., Lam, J. C., Lee, K. A., Miller, D., Oswald, J. E., Patel, N. C., Pukala, D. M., Quintero, O., Scaff, D. M., Van Snyder, W., Tope, M. C., Wagner, P. A., and Walch, M. J.: The Earth Observing System Microwave Limb Sounder (EOS MLS) on the Aura satellite, IEEE T. Geosci. Remote, 44, 5, 1075–1092, 2006.

Wiacek, A., Taylor, J. R., Strong, K., Saari, R., Kerzenmacher, T., Jones, N. B., and Griffith, D. W. T.: Ground-Based solar absorption FTIR spectroscopy: characterization of retrievals and first results from a novel optical design instrument at a New NDACC Complementary Station, J. Atmos. Ocean. Tech., 24, 3, 432–448, 2007.

Wood, S. W., Bodeker, G. E., Boyd, I. S., Jones, N. B., Connor, B. J., Johnston, P. V., Matthews, W. A., Nichol, S. E., Murcray, F. J., Nakajima, H., and Sasano, Y.: Validation of version 5.20 ILAS HNO_3, CH_4, N_2O, O_3, and NO_2 using ground-based measurements at Arrival Heights and Kiruna, J. Geophys. Res., 107, D24, 8208, doi:10.1029/2001JD000581, 2002.

WMO (World Meteorological Organization): Scientific Assessment of Ozone Depletion: 2006, WMO Global Ozone Research and Monitoring Project – Report No. 50, WMO, Geneva, 2007.

Yung, Y. L., Wang, W. C., and Lacis, A. A.: Greenhouse effects due to atmospheric nitrous oxide, Geophys. Res. Lett., 3, 10, 619–621, 1976.

Zander, R., Ehhalt, D. H., Rinsland, C. P., Schmidt, U., Mahieu, E., Rudolph, J., Demoulin, P., Roland, G., Delbouille, L., and Sauval, A. J.: Secular trend and seasonal variability of the column abundance of N_2O above the Jungfraujoch station determined from IR solar spectra, J. Geophys. Res., 99, D8, 16 745–16 756, 1994.

Zander, R., Mahieu, E., Demoulin, P., Duchatelet, P., Servais, C., Roland, G., DelBouille, L., De Mazière, M., and Rinsland, C. P.: Evolution of a dozen non-CO_2 greenhouse gases above central Europe since the mid-1980s, Environ. Sci., 2(2–3), 295–303, 2005.

Zander, R., Mahieu, E., Demoulin, P., Duchatelet, P., Roland, G., Servais, C., De Mazière, M., Reimann, S., and Rinsland, C. P.: Our changing atmosphere: evidence based on long-term infrared solar observations at the Jungfraujoch since 1950, Sci. Total Environ., 391, 184–195, 2008.